UCLA
UCLA Electronic Theses and Dissertations

Title

Internet of Things (IoT)-Enabled Health Monitoring Systems: Implementation and Validation

Permalink

https://escholarship.org/uc/item/747705sh

Author

Gwak, Migyeong

Publication Date

2022

Peer reviewed|Thesis/dissertation

UNIVERSITY OF CALIFORNIA

Los Angeles

Internet of Things (IoT)-Enabled Health Monitoring Systems:

Implementation and Validation

A dissertation submitted in partial satisfaction

of the requirements for the degree

Doctor of Philosophy in Computer Science

by

Migyeong Gwak

2022

ABSTRACT OF THE DISSERTATION

Internet of Things (IoT)-Enabled Health Monitoring Systems:

Implementation and Validation

by

Migyeong Gwak

Doctor of Philosophy in Computer Science

University of California, Los Angeles, 2022

Professor Majid Sarrafzadeh, Chair

Internet of Things (IoT)-based remote health monitoring (RHM) generates a paradigm shift from traditional healthcare services. RHM applications deliver healthcare solutions to the national and global demand of improving the health and wellness of the population. Recent advancements in sensing, computing, and network communication technology enable pervasive, cost-effective, and sustainable health monitoring. This dissertation introduces several IoT-enabled RHM applications in monitoring vital signs, physical movements, cognitive impairment, and mental health. Each RHM system is described in terms of the design of intelligent sensors, implementation of processing units, data analysis of the collected data, and validation with experimental results. As the IoT market size grows, the massive adoption of IoT-based RHM applications has the potential to improve the health and wellness of the population.

The dissertation of Migyeong Gwak is approved.

Xiang Chen

Yizhou Sun

Wei Wang

Majid Sarrafzadeh, Committee Chair

University of California, Los Angeles

2022

To God . . .

who gives me strength and inspiration

and

to my family (Jonggu Goag, Gwiyeob Kang,

Mihwa Kwag, Joon Hyoung Kim, and Hannah Hamin Kim)

for their unconditional love and support.

TABLE OF CONTENTS

LIST OF TABLES

ACKNOWLEDGMENTS

I would like to thank my advisor, Professor Majid Sarrafzadeh, for his generous support and intellectual guidance with enthusiastic supervision to explore various healthcare problems and innovative solutions. I also thank all my committee members, Professor Xiang Chen, Professor Yizhou Sun, and Professor Wei Wang, for their invaluable feedback.

I would like to gratefully acknowledge Ghazal Ershadi for her contributions to the literature survey, algorithm development, and experimental results in Chapter 3. I wish to express my gratitude to Professor Ellen Woo for her professional advice and feedback on the neuropsychological fields in Chapter 5. My appreciation also extends to Lionel Levine for his guidance in multiple mental health-related projects and his contributions to Chapter 6. Finally, I would like to give my special thanks to all collaborators in my research.

I also dedicate this dissertation to my many friends and the University Presbyterian Church family, who have supported me with prayers and encouragement during my Ph.D.

VITA

2014   B.E. (Engineering Physics), B.S. (Computer Science), and Minor (Mathe-
            matics), Murray State University.

2020   M.S. (Computer Science), UCLA.

2017–present Teaching Assistant, Computer Science Department, UCLA. Taught sec-
            tions of Computer Science M152A (Introductory Digital Design Labo-
            ratory) under direction of Professor Miodrag Potkonjak and Majid Sar-
            rafzadeh.

PUBLICATIONS

Ershadi, Ghazal, Migyeong Gwak, Afshin Aminian, Rahul Soangra, Marybeth Grant-Beuttler, and Majid Sarrafzadeh. Smart Insole: Remote Gait Detection Algorithm Using Pressure Sensors For Toe Walking Rehabilitation. In 2021 IEEE 7th World Forum on Internet of Things (WF-IoT), pp. 332-337. IEEE, 2021.

Gwak, Migyeong, Tyler Davis, Majid Sarrafzadeh, and Ellen Woo. Psychological Stress Detection in Older Adults with Cognitive Impairment Using Photoplethysmography. In 2021 IEEE 9th International Conference on Healthcare Informatics (ICHI), pp. 209-213. IEEE, 2021.

Levine, Lionel M., Migyeong Gwak, Kimmo Kärkkäinen, Shayan Fazeli, Bita Zadeh, Tara Peris, Alexander S. Young, and Majid Sarrafzadeh. Anxiety Detection Leveraging Mobile

Passive Sensing. In EAI International Conference on Body Area Networks, pp. 212-225. Springer, Cham, 2020.

Gwak, Migyeong, Ellen Woo, and Majid Sarrafzadeh. The role of ppg in identification of mild cognitive impairment. In Proceedings of the 12th ACM International Conference on PErvasive Technologies Related to Assistive Environments, pp. 32-35. 2019.

Gwak, Migyeong, Shayan Fazeli, Ghazaal Ershadi, Majid Sarrafzadeh, Melina Ghodsi, Afshin Aminian, and John A. Schlechter. EXTRA: Exercise Tracking and Analysis Platform for Remote-monitoring of Knee Rehabilitation. In 2019 IEEE 16th International Conference on Wearable and Implantable Body Sensor Networks (BSN), pp. 1-4. IEEE, 2019.

Gwak, Migyeong, Ellen Woo, and Majid Sarrafzadeh. The role of accelerometer and gyroscope sensors in identification of mild cognitive impairment. In 2018 IEEE Global Conference on Signal and Information Processing (GlobalSIP), pp. 434-438. IEEE, 2018.

CHAPTER 1

Internet of Things-Enabled Health Monitoring System

Internet of Things (IoT) technology has been matured and adopted in multiple domains, such as Industry 4.0, smart cities, smart homes, connected cars, and healthcare [DPR19]. McKinsey Global Institue describes the term IoT as *"the physical world is becoming a type of information system—through sensors and actuators embedded in physical objects and linked through wired and wireless networks via the Internet Protocol"* [LT13]. McKinsey also estimates *"IoT has a total potential economic impact of $3.9 trillion to $11.1 trillion a year by 2025"* [MCB15]. Furthermore, the number of IoT-connected devices is expected to reach 43 billion by 2023 across the world, which is an almost threefold increase from 2018 [DPR19].

The IoT applications in the healthcare sector are termed as Healthcare Internet of Things (H-IoT) [QNZ20]. The growing market size of IoT will lead more people to be connected by accessing IoT devices. Large-scale monitoring and massive adoption of H-IoT have the positive potential to improve the health and wellness of the population.

Remote health monitoring (RHM) plays a crucial role in H-IoT to link patients to their healthcare providers to provide end-to-end intervention. IoT-enabled RHM enables users to receive ongoing support related to general health and wellness outside the hospital utilizing technology. For example, a remote health monitoring system allows patients to transmit their vital symptoms to the healthcare system and receive medical feedback and treatment throughout the equipment and network. In addition, it enables healthcare providers to deliver quality care by continuously monitoring the patients' health conditions. Recent advanced technologies in sensing, modern communication, and data processing make RHM

systems accessible to consumers, patients, caregivers, and healthcare professionals.

The Coronavirus Disease 2019 (COVID-19) emergency has increased requests for upgrading healthcare delivery by telehealth visits and virtual networking. The COVID-19, the latest respiratory disease pandemic, is still plaguing global health because of its high rate of spreading infection [SDH20]. According to the descriptive statistics of complied survey results during the COVID-19 outbreak by [CKC21], 74% of Americans responded that they would like to use a telehealth service, and 84% wanted to receive a potential diagnosis from home to avoid risk around sick patients in the hospital. RHM applications can reduce physical contact or visiting healthcare facilities and effectively screen patients for COVID-19.

The larger aging population increasingly affects the socio-economic structure of society. The World Health Organization (WHO) estimates that people over 60 years of age in the global population will nearly double from 12% to 22% by 2050 [who]. As the 65 and older population continues to grow rapidly—it grew by over a third between 2010 and 2020 to total more than 54 million people—geriatric health issues will become even more prevalent. As people age, they become more susceptible to chronic conditions and injuries that significantly impact their lives. In fact, most adults over 65 in the United States live with two or more chronic conditions, such as heart disease, diabetes, or dementia. These conditions lead to a lower quality of life and are among the leading causes of death in seniors. Many chronic conditions require routine monitoring, which leads to numerous doctor's visits. An increased number of older adults will generate higher medical needs and caregiving, which may cause more pressure and burden on existing healthcare services [PRW21]. Total healthcare spending in the United States alone reached $3.6 trillion or $11,172 per person in 2018 [HMB20]. This amount indicates a 30.8% increase from healthcare spending in 2012. Given how expensive it is, millions of Americans go without healthcare every year; this only increases eventual costs tied to emergent health issues that could have been prevented. In fact, tens of thousands of people die in the U.S. as a result of not having healthcare coverage, with cost being the major factor for lack of coverage. In addition to saving money, reducing

healthcare costs saves lives. For the sake of social welfare, elderly healthcare, and well-being [MMD17], it is essential to implement a cost-effective and sustainable quality of care utilizing technology.

The planning direction of national and global health policymakers is toward utilizing more electronic health (eHealth) and mobile health (mHealth) applications to save possible healthcare expenses. For instance, the WHO focuses on providing interventions to clients, healthcare providers, resource managers, and cloud data services [PRW21]. Likewise, the National Health Services (NHS) updates the service model to boost digital-enabled, personalized 'out-of-hospital' care [PRW21]. Therefore, RHM applications are the most suitable solution for achieving policymakers' objectives.

IoT-enabled RHM is reshaping traditional healthcare services with many benefits. The advantages of remote patient monitoring include but are not limited to [MRD19, CKC21]:

- Early diagnosis and detection of diseases

- Ability to continuously monitor patients

- Real-time and personalized intervention, treatment, and drug management

- Prediction of forthcoming health issues

- Decreased healthcare cost and the number of hospitalizations

- Emergency medical care

- Efficient communication for healthcare services

- More accurate readings from the natural settings

- Improved patient experience and outcomes

1.1 System Architecture

Understanding the main components of an RHM system is an essential step to developing the application. An IoT-based RHM system is mainly comprised of three tiers: a things layer, a processing layer, and a communication layer [QNZ20].

The things layer involves various sensors or devices with embedded sensors, such as wearables, body implants, and environmental sensors, to collect the end user's health conditions. The body sensors measure multiple vital signs or physiological changes, such as heart rate, arterial oxygen saturation (SpO2), blood pressure, glucose level, respiration rate, body temperature, and electrodermal activity (EDA). In addition, tracking the user's motion is feasible via Micro-electromechanical systems (MEMS), including an accelerometer, gyroscope, pressure sensor, and magnetic field sensor. Sensing technologies enable sensors to be more advanced, more convenient to use, and more cost-effective. Non-invasive wearable sensors are required to be directly attached to the human body. Wearable sensors need to be comfortable, flexible, small in dimensions, chemically inert, non-toxic, and hypoallergenic [MMD17] because they directly contact the curvy and soft human skin. Commonly used H-IoT wearable devices exist in the form of fitness trackers [QNZ20], such as Apple, Fitbit, Garmin, and Whoop. Contactless methods in RHM have also been developed extensively over the past few years and allow the users to be present within a few meters from the sensors [MRD19]. Contactless RHM methods mainly use image or radio frequencies to detect the user's vital signs or physical activities by deploying the sensors to their home or accessing embedded sensors on personal devices (i.e., an RGB camera on a smartphone). Implantable sensors are invasive but can be more accurate in observing specific physiological parameters, like glucose level or neural activity [DM17]. Moreover, environmental sensors can measure air pressure, air quality, humidity, or ambient temperature of where the user lives. Changes in the living environment are also a good source of understanding the user's lifestyle and health conditions [PRW21].

The processing layer manages and analyzes the volume of data from the sensors or the things layer. The processing layer includes a processing unit/circuitry with data receiving and transmitting capability [MRD19]. The processing layer refers to the server-side, while the things layer represents the client-side [Alb21]. Implemented processing unit on the medical institute server enables extracting patients' health parameters and providing timely healthcare services by medical professionals. With emerging technologies, the processing unit utilizes feature extraction, decision support, big data analytics, machine learning, deep learning, natural language processing, and cloud computing [QNZ20].

The collected data from the things layer can be pre-processed at a local processing unit before being transmitted to the server or remote healthcare facilities, which is called an *edge node* in edge computing technologies. An edge node is a bridging point or a gateway between multiple body sensors and the server. The local processing unit on the edge node has been a Personal Digital Assistant (PDA), a microcontroller, a Field Programmable Gate Array (FPGA), or a personal computer [MMD17]. Recent RHM applications [CAE19, BSW15, WKF16, SZK15, JW15, GWS18a, LWZ16] focus on utilizing a smartphone as a gateway due to the increased number of users and the recent advances in communications and processing capabilities. Users can carry their smartphones whenever they go to break the time and location barrier of the activity assessment.

The communication layer connects the things and processing layers utilizing wireless technologies. The critical feature of IoT is Wireless Sensor Networks (WSNs), and IoT in the healthcare sector focuses on the Body Sensor Networks (BSNs), personal area network (PAN), or Wireless Body Area Networks (WBANs) [QNZ20]. In the review paper by Philip et al., the WBAN based on the IEEE 802.15.6 standard is *"developed for enhanced health monitoring, which supports data rates up to 10Mbps, 1-2 meters range, low power, and high reliability"* [PRW21]. In the things layer, a short-range network protocol, such as Bluetooth, ZigBee, ANT, Near Field Communications (NFC), RFID, and WiFi, allows communications between body sensors and a gateway [MMD17]. BLE can transmit sensor signals with a low

bandwidth of 0.5 Hz, while WiFi is required for the high bandwidth of 500 Hz [PRW21].

This dissertation presents the implementation of five IoT-enabled RHM systems, mainly focusing on developing better devices and data processing pipelines in the things layer and processing layer, respectively. Each system is described in terms of design, implementation, experiment, result, validation, and challenges. Emerging RHM applications have positively impacted treating several cardiovascular, neurological, pulmonary diseases, diabetes, mobility issues, and more [MRD19]. This dissertation includes RHM system validation in monitoring vital signs, physical movements, and mental health. The rest of this dissertation is organized as follows. A motion-based respiratory rate estimation using a video recording of the face and upper body is introduced in Chapter 2. A real-time intervention to prevent toe walking is shown in Chapter 3. A remote exercise tracking tool after a knee reconstruction surgery is presented in Chapter 4. A clinical assistive tool to identify cognitive impairment utilizing physiological and physical changes is introduced in Chapter 5. Mental health monitoring with passive sensing of a smartphone is discussed in Chapter 6. Some of these RHM applications still require further development and analysis. Finally, Chapter 7 presents future research directions and the conclusion.

CHAPTER 2

Camera-based Respiration Rate Estimation

2.1 Objectives

Respiratory rate (RR) is a significant vital sign indicating overall respiratory dysfunction and a biomarker for respiratory system functionality and wellness. Monitoring of RR is beneficial for patient care, especially for the ones with asthma, congestive heart failure, cardiac arrest, and breathlessness due to infection [ILC19, KMO21]. RR is a reliable predictor of intensive care admission and death [PHV17].

RR is also an objective and pre-clinical marker in the latest respiratory disease pandemic, Coronavirus Disease 2019 (COVID-19). Unlike other viral illnesses such as influenza or the common cold, a lower-respiratory tract infection appears in most COVID-19 cases, which cause inflammation of lung tissue, coughing, and shortness of breath [SDH20]. Thus, RR increases from the baseline to compensate when the overall efficiency of the lungs is reduced by COVID-19 [SDH20].

Estimating RR using on-body sensors offers a non-invasive way to remotely monitor an individual's health conditions. Wearable sensors are expected to directly attach to the individual's body, like the face, torso, wrist, or finger. Available commercialized devices for respiration monitoring include a chest belt, face mask, fingertip oximeter, nostril sensor, and wrist band. However, physical contact-based measurement is not appropriate for the population with sensitive skin, such as premature neonates and the elderly [BDG13]. It is also cumbersome for patients who need to wear these instruments for long-term monitoring.

In addition, sharing contaminated measuring devices pose an extreme risk of spreading the disease within hospitals and assisted living facilities. Therefore, contactless respiration monitoring is growing interest.

A contactless RR measurement can be obtained using wireless signals, such as acoustic [IRA21] or radio-frequency signals [SHZ20]. The respiration state is acquired by receiving a continuous propagated wave, which is influenced by repetitive chest movement while breathing. Especially, ultra-wideband (UWB) radar-based system has been used to detect respiration patterns of multiple persons [YCL19]. However, a RR estimation using wireless signals often has a limitation: the signal emitter should be located close to the human body, and the measurement is mainly optimized for indoor settings. Camera-based respiration monitoring is not restricted to personal mobility and is an alternative solution with recent advances in camera technology and image processing techniques.

Infrared thermography, also known as thermal imaging, is one method of camera-based respiration monitoring. Infrared thermography captures radiation naturally emitted from the human skin and does not need any light source [PHV17]. Several studies validated that infrared spectrum analysis can detect the prevalence of respiratory activity that causes temperature modulation at the nostrils of preterm infants [PHV17] and patients receiving general anesthesia [HBL18]. However, a thermal camera is often expensive and usually not available on personal consumer-level devices.

Using a standard RGB camera is another method of camera-based RR estimation due to the subtle color variations of the human skin's surface. According to Respiratory Sinus Arrhythmia (RSA) phenomenon, heart rate increases during inspiration and decreases during expiration, so RR can be derived by measuring pulsatile activity [SDH20]. Photoplethysmography (PPG) signal is proportional to the quantity of blood flowing through the blood vessels. While conventional PPG makes measurements at the skin surface, the changes in blood volume can be detected by analyzing subtle, momentary changes in skin color, known as remote PPG (rPPG). The skin color measured by a camera changes over time due to blood volume.

Algorithmic principles behind rPPG analyze the temporal RGB value changes of skin pixels to extract the pulse signal [WBS16]. Pulse extraction of the existing rPPG methods can be achieved based on principal component analysis (PCA) [BDG13, INM14], independent component analysis (ICA) [SY13], chrominance signal [DJ13], or a plane orthogonal to the skin tone (POS) [WBS16]. PCA or ICA-based methods are statistical approaches to separate RGB signals into multiple source signals, including the pulse signal. However, the extracted pulse signal may not exploit unique skin reflection properties for each individual. In this regard, the chrominance signal-based method defines the standardized skin-tone vector, and the POS-based method defines the projection plane by using the data-driven approach to eliminate skin-tone variation to the projection direction [WBS16]. Still, the rPPG method using a color variation on the skin pixels is vulnerable to the various illumination spectra and intrinsic skin tone. Moreover, the rPPG method is tricky to apply to the population with various measurements because the skin tissue must be visible to the camera.

This chapter focuses on estimating RR based on subtle motion captured from a video with the subject's face and upper body. Because the chest movement due to breathing provides more robust estimation accuracy, adaptive selection between the face and chest regions is proposed depending on the visibility of each region. Motion-based RR measurement does not require direct assessment of thermal or skin-color changes. It allows estimating RR from individuals with various conditions with clothing and face-coverings, such as eyewear, face mask, hijab, hat, or heavy makeup. However, motion-based RR estimation is vulnerable to the subject's excessive voluntary physical movement. Therefore, we propose a robust motion artifact removal technique to extract cleaner respiratory signals from the tracked motion signal. Frontal face RGB video recording is prevalent on personal devices, such as laptops or smartphones, enabling mobile and instantaneous RR monitoring daily.
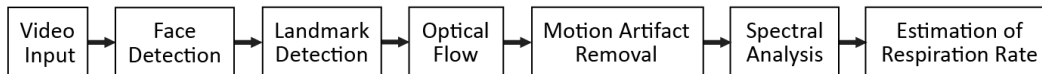
Figure 2.1: Proposed framework for extracting RR.

2.2 Related Works

Tracking the movement of the chest, abdomen, or shoulder is one of the methods to monitor respiration. Janssen et al. [JWM15] focused on automatically detecting a region of interest (ROI) on the chest or abdomen from the pixel motion vectors by the dense optical flow algorithm and extracting the respiratory signal from other motion sources via motion factorization. They evaluated the performance of their video-based respiration monitoring system through 148 video recordings from four adults and two neonates. Tveit et al. [TEA16] designed a respiration detection algorithm using the global motion signal, which was based on the variation in the local phase from the first frame of the video. Their phase-based algorithm was tested on six video recordings of two babies on the bed. It showed more invariance towards different ROI selections (i.e., the trunk or entire body of the baby) than pixel intensity-based motion tracking. Lin et al. [LCT16] characterized the vertical motion by detecting Haar-like features on the neck and chest region in the energy map and tested on 296 video recordings from 11 adults with sitting posture. Direct assessment of the chest movement provides reliable RR measurement results. However, these approaches are not suitable to apply in a real-time respiratory monitoring system because the chest, abdomen, or even shoulder may not always be visible in a video recording during daily activities.

In this regard, respiratory rate estimation from the subject's frontal face videos has attracted much attention in recent years. Schrumpf et al. [SMB19] averaged the pixel values of each RGB color channel to extract the motion-based respiratory signals from both face and upper chest regions and estimated the RR leveraging the empirical mode decomposition. They validated with 12 subjects that derived motion signal from the facial region is correlated with breathing movement of the chest and can be an alternative to rPPG-based RR estimation. Iozza et al. [ILC19] exploited head movements to identify motion artifacts in the rPPG system and found the performance is mainly appropriate for medium respiratory frequencies with the video recordings from 20 subjects. Finally, Mehta and Sharma [MS20]
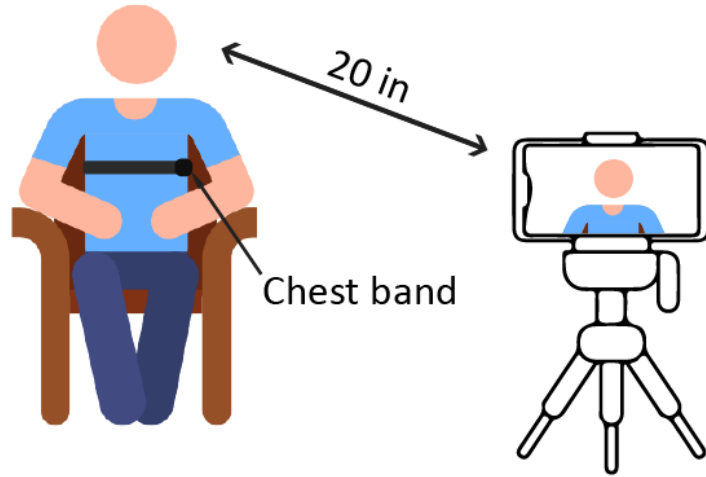
Figure 2.2: Illustration of the experiment setup.

conducted a study to track the movement at the nose tip via optical flow using data from 13 subjects in the DEAP dataset [KMS11], which is a publicly available dataset including frontal face videos and physiological signals. They achieved the mean absolute error of 2.94 ± 2.13 breaths per minute. Still, accurate detection and tracking of nostril movement may not be feasible when the subject is covering their face with a mask, commonly used for preventing the spread of germs and viruses (e.g., COVID-19). Another limitation in the studies is that the dataset used for validation is too small to generalize the measurement over a broader population.

Existing motion-based RR measurement methods had the challenge of directly using subtle head motion, which is vulnerable to subjects' voluntary head movement. However, the head-neck system is biomechanically connected to the trunk, and unconstrained head motion can occur as a result of chest motion [BDG13]. Therefore, the chest movement can induce involuntary respiratory-related head motion due to breathing when the subject is stable. In the scenario of using an RGB camera on personal devices, the head or upper chest motion-based instantaneous RR measurement is achievable with a front-facing video in real-time.

2.3   Method

We present a robust, cost-effective, non-contact respiration monitoring system by tracking the movement of the head or upper chest using an RGB camera. Our system adaptively selects landmarks on the face or upper chest regions based on their visibility in the video recordings to obtain the respiratory-induced motion signal. Then, a respiratory signal is derived from the motion signal and cleaned by removing large movement artifacts. Our system uses power spectrum density and signal-to-noise ratio to calculate instantaneous RR every second from the derived respiratory signal.

2.3.1   Experimental Setup

Thirty healthy subjects with diverse skin tones were involved in the data collection. The Institutional Review Board (IRB) approved the study, and the subjects provided their consent to collect their data. During the visit, the subject was asked to fill out a questionnaire to provide demographic information and the Fitzpatrick skin phototype [Sac09]. Video recordings were collected with a Samsung Galaxy S21 Ultra smartphone. The resolution was set to full HD 1920x1080 at 60 frames per second (fps). The subject was sitting on a chair and looking at the smartphone camera from a distance of 20 inches and kept the face devoid of any motion as much as possible. The subject was wearing a face mask during the visit. The experiment room and equipment were sanitized before each use by the subjects to prevent the spread of viruses. Each video recorded the subject's face and upper chest with a white background.

- **Natural Breathing**: First, the subjects were asked to perform regular and natural breathing through the nose only ("Nose InOut") with the preferred pace. Then, the subjects were asked to perform another natural breathing through the mouth only ("Mouth InOut"). Their video and reference data were recorded for 1.5 minutes for each task.

- **Controlled Breathing**: Subjects were asked to maintain their breathing at five different rates: 5 breaths per minute (BPM), 10 BPM, 15 BPM, 20 BPM, and 25 BPM. Video animations illustrating cycles of breathing were provided for the subjects to guide their breathing and help them maintain the rate during the recording. Their video and reference data were recorded for 1 minute for each reference respiratory rate.

The reference respiratory signal was recorded by Zephyr Technology's BioHarness chest band, which measures chest expansion and contraction using the tension on the strap. The reference respiratory signal was synchronized with each video recording based on the timestamp. The ground truth RR was extracted from the respiratory signal by calculating the distance between consecutive peaks and then sampled for every second using linear interpolation.

2.3.2 Motion Signal Extraction

In our contactless respiration monitoring system (Fig. 2.1), face detection is the first step to obtaining head or chest motion signals. The face detection step searches for the rectangular region of the face in the initial frame in the input video. If a face region is not available in the first frame, the system iterates the successive frames until finding one. Deep learning-based face detection from OpenCV, pre-trained with ResNet-10 architecture as the backbone in TensorFlow, is applied for this step. Another prevalent approach for face detection is the Viola-Jones algorithm [VJ01], which identifies the difference in brightness between the rectangles over a specific area, such as eyes, mouth, and the bridge of the nose. However, face detection using a deep learning model performs better than the Viola-Jones algorithm in our dataset, in which a face mask covers the subject's mouth and nose area.

Adaptive landmark selection is the next step before tracking the motion signals. As discussed in the previous section, respiration-induced chest movement provides a less vulnerable respiratory signal than face movement. However, the chest, abdomen, or shoulder

is not always visible during the facial video recording. Therefore, our method adaptively selects landmarks either on the chest or face region based on the visibility of the subject's upper chest in the input video.

The chest region is recognized based on face detection. First, the face length was calculated from the rectangular face region. If $\frac{1}{10^{th}}$ of that length below the face region is obtainable inside the frame boundary, it is considered as the position of the chest landmark (a green circle in Fig. 2.3); then, the point is followed to track the upper chest motion. Our method identifies 68 landmarks in the face region using OpenCV's Local Binary Features (LBF565) [RCW14] face alignment model if the chest landmark is not located within the frame boundary. Only nine facial landmarks (the blue triangles in Fig. 2.3) out of 68 are selected on the nose bridge and both sides of the cheekbone, which are less likely to be interrupted by facial expressions or eye blinking to track the head motion.

The horizontal (X-axis) and vertical (Y-axis) movements of the selected landmarks were tracked by the Lucas–Kanade–Tomasi (LKT) optical flow algorithm [TK91]. The LKT algorithm detects the location of the landmarks along the X-Y coordinate in every video frame. The motion signals correspond to the landmark's location changes within the video recording with a fixed camera. Tracking the landmark sometimes stops when the feature point moves beyond the frame boundary due to the subject's voluntary movement. In this case, our method searches for the face or chest landmarks again to continue motion signal extraction.

An overlapping sliding window approach is used to estimate RR every second. The motion signals are initially buffered for 30 seconds, and the 30-second window slides with a 1-second step size. Then, each window is processed to remove motion artifacts and measure instantaneous RR per second.

2.3.3 Motion Artifacts Removal

A respiratory signal can be induced from the involuntary head or chest motion. However, it is often vulnerable to noise due to sudden voluntary physical movement during a video recording. A motion artifact removal step is required to obtain a clean respiratory signal in the motion-based RR estimation. Two motion signals are processed to extract a respiratory signal: a Y-axis motion signal and a magnitude signal. A magnitude signal is calculated from the X and Y-axis motion signals using equation (1). In motion artifact removal, at first, the motion signal is smoothed with a moving average. Then, motion speed is evaluated by calculating the differences between successive values in the motion signal using equation (2) since the video frame rate is constant as 60 fps. Finally, the absolute values of the speed signal are used to define a threshold for motion artifact removal.

$$mag[n] = \sqrt{x[n]^2 + y[n]^2} \tag{1}$$

$$mag'[n] = mag[n] - mag[n-1] \tag{2}$$

Sudden motion artifacts have a higher speed than the respiratory-induced motion of the head and chest. Therefore, the artifacts appear as outliers in the distribution of the absolute speed signal. We utilized kurtosis to determine if a 30-second window motion signal has sudden motion artifacts. If kurtosis is bigger than 3, the motion signal is more likely to have outliers because kurtosis of the normal distribution is 3.

After identifying the existence of motion artifacts, the outliers can be determined by a static or dynamic threshold. We manually selected 0.35 as a static threshold based on our observation of the distribution of magnitude signal values. The top 10 percent of the distribution of the absolute speed signal in the Y-axis became the dynamic threshold in each window. Only the speed signal in the Y-axis is used since respiration mostly affects the vertical movement of the face or chest. Any motions in the X-axis are more likely to be

noise during a voluntary motion. Therefore, a Y-axis speed value beyond the threshold is considered an outlier and is replaced to zero, similar to replacing sudden movements with breath-holding.

If sudden motion artifacts are not recognized, our method leverages the speed of magnitude signal in addition to the Y-axis speed signal. The magnitude signal magnifies involuntary head or chest motion when the subject is not vertically aligned to the camera. In addition, the magnitude signal mitigates the sensitivity of the moving direction because it combines two motion signals in X and Y coordinates. Finally, the cleaned signal after motion artifact removal is used to estimate RR.

2.3.4 Respiratory Rate Estimation

The spectral analysis is used to estimate an instantaneous RR. Our method first removes the linear trend of the cleaned speed signal. Then, the moving average technique makes the signal smooth. The Butterworth filter with cut-off frequencies of $f_{c1} = 0.1$ Hz and $f_{c2} = 3$ Hz using the Hamming window extracts the signal within the frequency spectrum related to breathing. The filtered signal corresponds to a respiration signal in a 30-second window. The respiration signal is normalized by the Frobenius norm and converted by the discrete Fourier Transform (DFT) with zero padding. Our method estimates RR from 3 to 30 BPM from the frequency-domain signal to avoid excessively incorrect estimation. The frequency component with the highest peak corresponds to the instantaneous RR by observing the DFT signal. Instant RR is measured for all the landmarks accordingly. Signal-to-noise ratio (SNR) can determine the highly correlated signal waveform to respiration. Therefore, a RR with the highest SNR is selected among measured RRs from multiple landmarks.

In summary, Fig. 2.4 depicts an example of signal processing and motion artifact removal of our method. The top two waveforms are the raw tracking signals in the X and Y-axis by the LKT algorithm. An abrupt change is clearly observed in the middle of the signal due to the subject's voluntary head movement. The third chart is the magnitude signal, while the

16

fourth chart is the speed of the magnitude signal, which is the same as differentiation. The differentiation makes the waveform around zero but keeps the abrupt changes. The absolute of the speed signal is helpful to determine outliers, as shown in the fifth chart. Our motion artifact removal defines and withdraws outliers based on a threshold. Then, a band-pass filter converts the clean signal into a respiration signal (the sixth chart in Fig. 2.4). The respiration signal has 11 peaks corresponding with 11 inhalations in a 30-second window. Moreover, the respiration signal has an almost flat pattern where the outliers appear, like holding a breath while having a voluntary movement. An instantaneous RR is calculated from the frequency with the highest peak in the power spectrum.

2.4 Results

The performance of the proposed method was evaluated using 210 video recordings. The measured value, RR_{est}, is compared with the ground truth, RR_{ref}, acquired using the chest band. The accuracy is evaluated by mean absolute error (MAE) using the following formula.

$$MAE = \frac{1}{N} \sum_{n=1}^{N} |RR_{est} - RR_{ref}| \tag{3}$$

Table 2.1 represents MAE and standard deviation of head and chest motion-based RR estimation with our dataset at 60 fps. The table also shows the experiment results of controlled breathing tasks with five different respiratory rates from 5 BPM to 25 BPM and natural breathing ("Mouth InOut" and "Nose InOut"). The rightmost column ("None") in the table represents the error for the scenario without using the motion artifact removal technique, which is a baseline to compare the results of using motion artifact removal based on a static ("Static") or dynamic ("Dynamic") threshold. Our facial video recordings are administered to record the upper chest area of all 30 subjects. Our adaptive landmark selection will only select the chest region in our dataset because chest motion-based RR measurement always gives better results than head motion-based measurement. Two result

Table 2.1: Mean absolute error and standard deviation of motion-based respiratory rate (in BPM) with motion artifact removal using dynamic and static threshold and without motion artifact removal ("None") in 60 fps

Head Motion			
Tasks	Dynamic	Static	None
5 BPM	4.17(2.32)	4.49(2.68)	4.39(2.62)
10 BPM	0.82(1.06)	1.05(1.37)	1.07(1.37)
15 BPM	0.78(0.70)	0.96(0.82)	1.03(0.89)
20 BPM	1.24(1.47)	2.59(2.38)	2.36(2.11)
25 BPM	2.60(4.26)	3.29(5.2)	3.26(5.10)
Mouth InOut	2.05(2.69)	2.57(3.02)	2.56(3.00)
Nose InOut	1.98(1.60)	2.36(1.86)	2.33(1.87)
Total	1.95(1.19)	2.47(1.23)	2.43(1.18)

Chest Motion			
Tasks	Dynamic	Static	None
5 BPM	2.26(2.16)	3.11(2.27)	3.12(2.28)
10 BPM	0.60(0.66)	0.56(0.60)	0.55(0.60)
15 BPM	0.58(0.43)	0.60(0.41)	0.65(0.52)
20 BPM	0.83(0.65)	1.03(1.04)	1.12(1.47)
25 BPM	1.95(4.44)	2.78(5.03)	2.80(5.06)
Mouth InOut	1.38(1.28)	1.50(1.38)	1.50(1.38)
Nose InOut	1.36(1.08)	2.24(2.10)	2.26(2.10)
Total	1.28(0.66)	1.69(1.04)	1.71(1.03)

tables allow us to estimate the performance of adaptive landmark selection whether the subject's chest region is available or not.

The results validate that our method successfully estimates RR for different respiratory rates and removes nonrespiratory noise from captured motion signals. The dynamic threshold technique achieves the best performance. The average MAE is 1.95 ± 1.19 BPM using head motion only and 1.28 ± 0.66 BPM using chest motion only. Motion-based RR estimation with a static threshold technique and without motion artifact removal are similar in performance. Estimating regular breathing frequency (10 or 15 BPM) outperforms other breathing frequencies. The highest measurement error occurs on the slow breathing frequency (5 BPM) task. The measured RR is always higher than the actual RR for the 5 BPM controlled breathing task because differentiation in one axis amplifies high-frequency components. The measurement of fast breathing (20 or 25 BPM) has a relatively higher error because our study participants had more voluntary movement during the fast breathing recording.

As discussed in the related work section, Mehta and Sharma [MS20] tested head motion-based RR estimation with the DEAP [KMS11] publicly available dataset, which is mainly for investigation of human affective states. The dataset measures the natural breathing rate throughout emotional stimuli to observe physiological changes. Their reported MAE was 2.94 ± 2.13 BPM, which is much higher than our result.

A higher video frame rate maintains motion details but is not always available with all of the RGB cameras on personal consumer-level devices. Our video datasets were recorded with a frame rate of 60 fps. We obtained motion tracking at lower video frame rates by dropping the frames. Table 2.2 shows MAE and standard deviation of our method using a motion artifact removal with a dynamic threshold at 30 fps and 15 fps. The average MAE for each frame rate is similar to the result with 60 fps but still better than the approach without motion artifact removal from Table 2.1. This result verifies that our method accurately measures RR with various video frame rates. Moreover, it validates that high FPS may not

be required for video-based respiration rate monitoring.

We compared the estimated averaged RR of each video with the averaged ground truths. Correlation plots of motion based on both face and chest regions are shown in Fig. 2.5. The Pearson correlation coefficient between the measured and the ground truth is 0.886 for head motion and 0.934 for chest motion. The p-values for respiration rate estimation from both motion signals are less than 0.05. A Bland-Altman plot [BA99] represents the difference between estimated RR and ground truth RR, $RR_{est} - RR_{ref}$, about the mean of both measurements. As shown in Fig. 2.6, the mean of the difference is very close to zero for both regions, although chest motion-based RR has a smaller standard deviation of the difference than face motion-based RR.

2.5 Conclusion

This study introduced a robust RR estimation method based on movement associated with respiration. Existing motion-based RR measurement approaches were vulnerable to subjects' sudden, voluntary movement, which is noise to obtain a clear respiratory signal. To the best of our knowledge, there is no related work focusing on deriving RR solely from the head motion. Results validate that our motion-based RR estimation with a motion artifact removal measures instantaneous RR with high accuracy. Furthermore, adaptive landmark selection between the chest and face regions benefits various facial video recordings with a smartphone camera in the natural setting. Our framework can support people with the capability to monitor breathing rates throughout their everyday lives continuously.
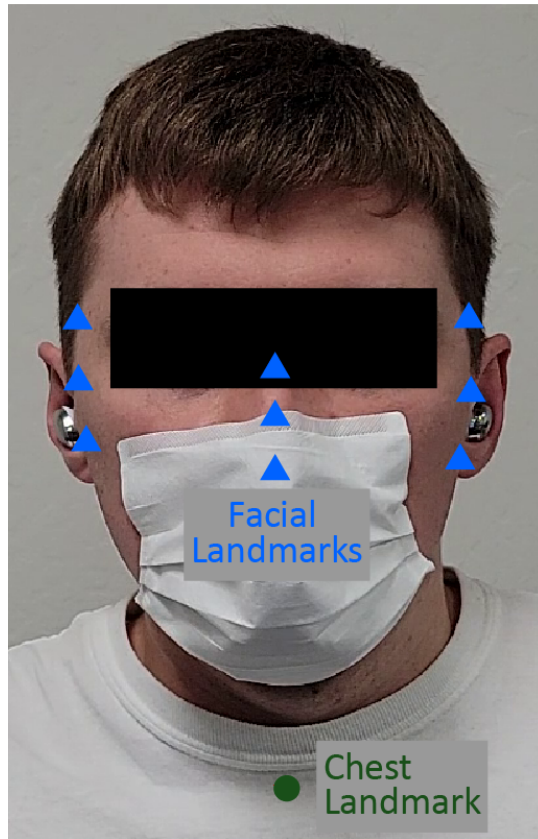
Figure 2.3: Illustration of face and chest landmarks identified in a frame of the video.
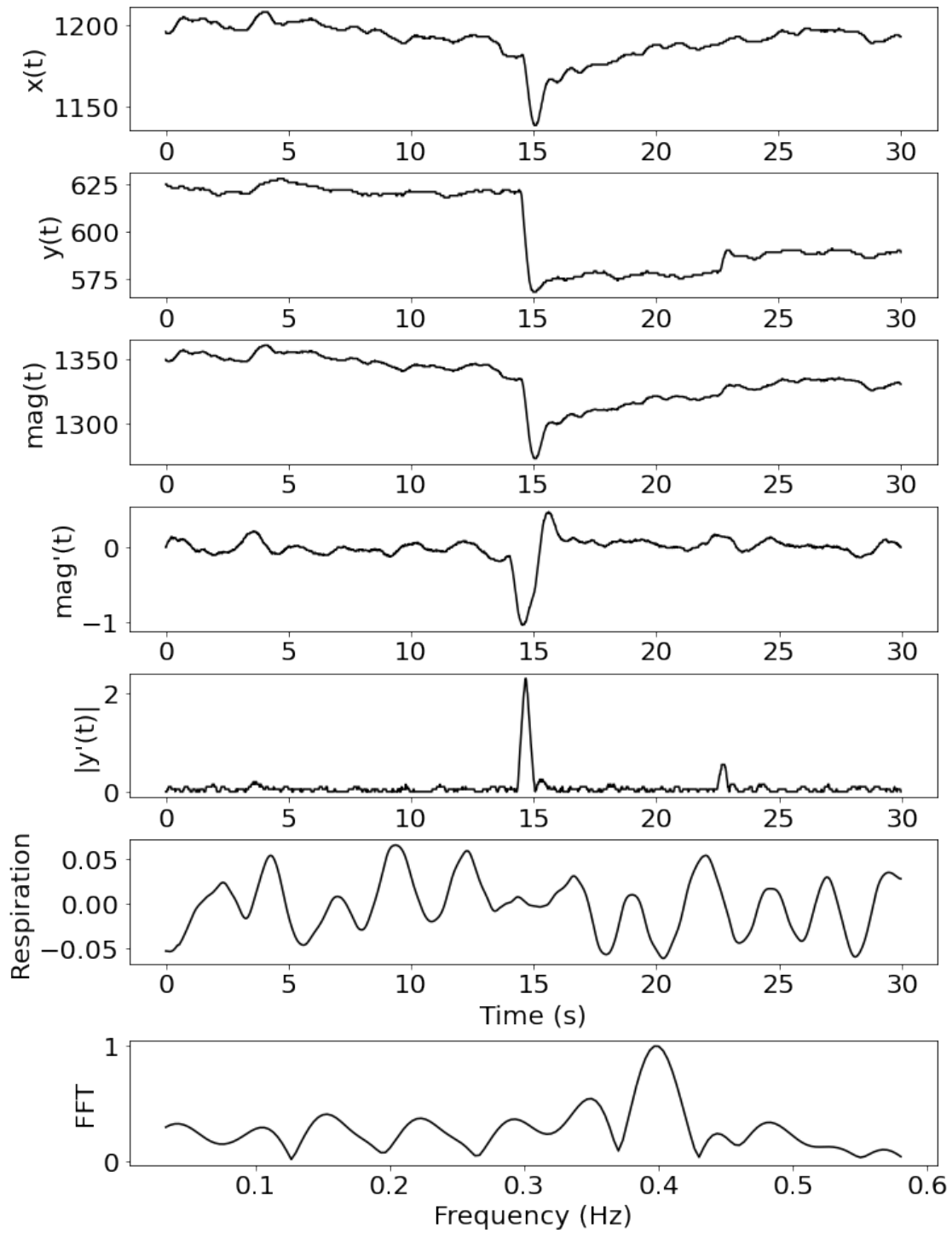
Figure 2.4: An example of signal processing and motion artifact removal of the proposed method

Table 2.2: Mean absolute error and standard deviation of motion-based respiratory rate (in BPM) using dynamic threshold technique in 30 and 15 fps

Head Motion		
Tasks	30 fps	15 fps
5 BPM	4.09(2.18)	3.98(2.12)
10 BPM	0.90(1.10)	0.89(1.04)
15 BPM	0.80(0.71)	0.73(0.57)
20 BPM	1.43(1.75)	1.25(1.52)
25 BPM	2.43(4.07)	2.47(4.13)
Mouth InOut	2.30(2.98)	2.19(2.53)
Nose InOut	1.88(1.45)	1.80(1.38)
Total	1.98(1.13)	1.90(1.12)

Chest Motion		
Tasks	30 fps	15 fps
5 BPM	2.22(2.12)	2.15(2.17)
10 BPM	0.58(0.62)	0.68(0.82)
15 BPM	0.62(0.56)	0.57(0.39)
20 BPM	0.84(0.65)	0.85(0.65)
25 BPM	1.97(4.44)	2.19(4.64)
Mouth InOut	1.36(1.22)	1.41(1.39)
Nose InOut	1.36(1.11)	1.30(1.10)
Total	1.28(0.64)	1.31(0.66)
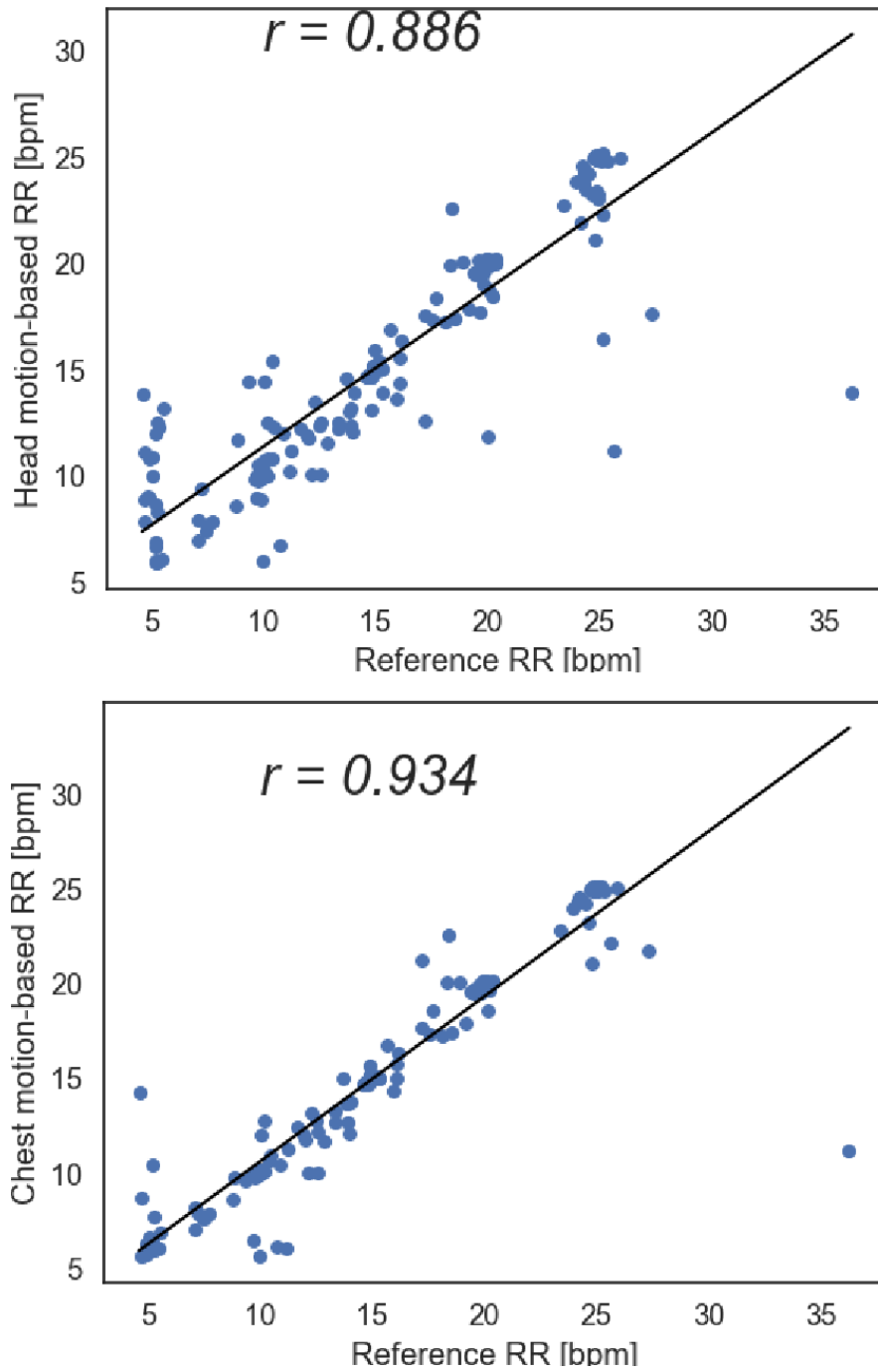
Figure 2.5: Correlation plots of the head motion based RR (top) and chest motion based RR (bottom) against reference RR from the chest band
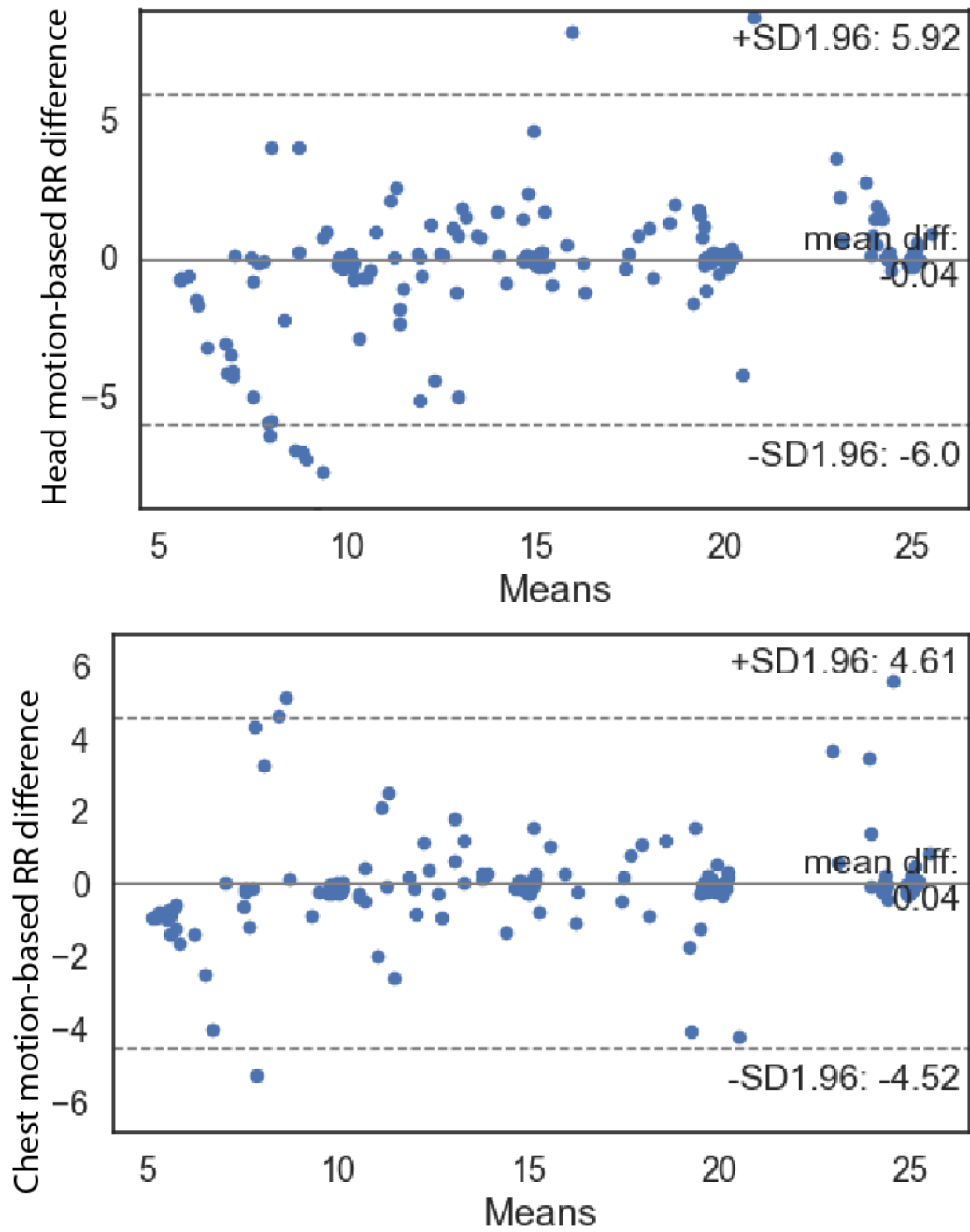
Figure 2.6: Bland–Altman plots of the head motion based RR (top) and chest motion based RR (bottom)

CHAPTER 3

Real-time Intervention to Toe Walking

3.1 Objectives

Toe walking is a gait pattern where a person walks on the toes or balls without the heel touching the ground during the gait cycle. Toe walking is one example of gait abnormality defined by a decreased range of ankle movement [LWM06]. Toe walking is commonly observed among toddlers starting to learn how to walk. After the toddler years, most children grow out of walking on their toes and begin to walk normally with the heel to toe pattern [SSK99]. Toe walking is associated with several diagnoses, such as a short Achilles tendon, muscular dystrophy, cerebral paralysis, and autism spectrum disorder [SSK99]. When growing children persist in toe walking with no signs of neurological, orthopedic, or psychiatric disease, and the cause of toe walking remains unexplained, they are diagnosed with idiopathic toe walking (ITW) [HW04, SSC97]. A child with ITW habitually walks on the forefoot, but they can perform heel-to-toe walk for short periods when they are asked to do so [WTC10, HW04]. The incidence of ITW has been estimated at 7% to 24% of the childhood population [EGU11].

Persistent toe walking may manifest foot deformities, ankle dorsiflexion limitations, poor alignment of posture, and impaired balance [RSD16, GH01, HMR07], but is often difficult to cure with traditional treatments. A serial casting on the foot and ankle has been proved to be a reduction in toe walking severity in [LBS04, DBH18]. Still, many other studies [SA98, EMD00] report that conservative treatments do not have any lasting effect on toe walking.

In [WPB16], Botulinum toxin (BTX-A) has the capability of reducing the development of plantar flexion torque. However, research in [SBO16] found out injecting BTX-A did not significantly decrease toe walking after 24 months of follow-up. Surgical tendon lengthening is a surgical treatment to toe walking [EMD00], but the reported failure rate is over 30% [HW04]. Other possible treatment methods to keep adequate ankle dorsiflexion include gait retraining [CSY10], stretching exercises, and ankle-foot orthoses [SA98]; however, the sustainability of the beneficial effects of these treatments appears to be brief. More promising analyses and interventions of ITW still need to be developed and validated.

Variability of gait parameters has been an indicator of health, such as Parkinson's disease [ZXL19], cardiovascular disease [MGM14], fall detection [BGM08], and cognitive decline [GWS18b]. Gait analysis has been used to monitor patient progress in orthopedics and rehabilitation [AYV18]. A gait cycle (or stride events) contains a stance phase (initial contact, loading response, mid stance, terminal stance, and pre-swing) and a swing phase (initial swing, mid-swing, and terminal swing) [AYV18]. Information about human locomotion includes quantitative measures (i.e., length, speed, and angle) of step, stride, stance, and swing. The traditional clinical assessments to analyze gait parameters rely on subjective or semi-subjective scales [AYV18]. Subjective gait assessment tools, such as the Gait Abnormality Rating Scale [BV02], Four Square Step Test [DE13], and Functional Gait Assessment [WK10], are more likely to have observer variations which affect the accuracy of diagnosis [AYV18]. Objective measurement to characterize human gait is obtainable through advancements in technology, including instrumented walking mats, treadmills, and motion capture systems [MGM14]. These instruments are often expensive, difficult to use, and require a clinical setting to be installed and measured. Moreover, these devices do not support portability or real-time feedback while the patients walk outside the clinics.

A real-time assessment system enables real-time intervention. Because ITW is a habitual or behavioral activity among healthy children, behavior change techniques (BCTs) [AM08] may motivate them to put their heels down while they are walking. Based on control theory

[CS82], designing a system to record walking activities to compare the daily number of toe strikes and heel strikes can bring positive outcomes to the individuals with ITW. The remote assessment system can prompt a specific goal setting (i.e., achieving more heel strikes) and provide an intuitive interface to review the goals compared to the recordings. These children may not need conservative or surgical treatments with high-cost clinical visits to overcome ITW. The system with wearable sensors can detect continuous toe walking and give just-in-time adaptive intervention (JITAI).

We introduce a remote toe walking monitoring system, GAIToe (**G**ait **A**nalysis utilizing an **I**nertial measurement unit (IMU) for **Toe** walking detection and intervention). The GAIToe uses a single IMU in an insole to detect physical activities: toe walking, heel-toe walking, standing on the toe, normal standing, sitting on the toe (sitting heel raises), and normal sitting. The GAIToe vibrates when it detects toe walking, toe standing, and toe sitting. The vibrations can be turned off with a heel strike, encouraging continuous heel strikes to prevent toe walking. In addition, the Bluetooth capability on the GAIToe sends data to an Android app, which displays the number of strides in real-time so that the users can review their walking patterns and progress anytime and anywhere. Our goal of this system was to provide real-time feedback while the user is walking with or without an Internet connection. Therefore, we focused on developing edge computing. We embedded all computation for activity recognition and device operation on the microcontroller. A smartphone was the network hub between the insoles and the cloud and provided local storage and data visualization. We used cloud storage services to save the data only whenever the smartphone was connected to the Internet.

3.2 Related Works

Multiple gait monitoring systems have been proposed to provide information about human locomotion and foot movements by equipping sensors in the shoe or insole. Xu *et al.* [XHA12]

proposed a smart insole to compute gait parameters with 48 pressure sensors, an accelerometer, a gyroscope, and a compass. Lin *et al.* [LWZ16] presented a smart insole that measures plantar pressure with an array of piezoelectric sensors and movement information with inertial sensors. Both studies developed smartphone software for data processing and real-time computing. Sazonov *et al.* [SFH10] utilized five force-sensitive resistors (FSRs) placed on an insole and an accelerometer positioned on the back of the shoes. Their sensor system recognized human body posture and activity by employing support vector machines (SVMs). Hegde *et al.* [HZU17] proposed a pediatric smart shoe system for remote activity (sitting, standing, and walking) detection. They placed five FSRs and an accelerometer on the insole and mounted other controller and data transmission components on the back of the shoes. FootMoov [CLT16], a commercial smart shoe by Carbonaro *et al.*, achieved the detection of the gait phases (heel-strike, stance, heel-off, and swing) utilizing two FSRs located on the heel and forefoot and an accelerometer embedded in the forefoot. All of these works are useful to track human locomotion and walking status. However, their complicated systems and algorithms are not explicitly designed for toe walking detection and interventions. Also, most of these gait monitoring systems depend on smartphone software for data acquisition, storage, and processing.

Our proposed platform, GAIToe, detects different walking, sitting, and standing behaviors by integrating a single IMU in an insole. We selected an IMU because the shoes' acceleration data were sufficient to identify different gait patterns based on the literature and our experiments. The system costs less than $80.00 before the cost-saving of mass production. The sensor unit is not exposed and does not deform the exterior design of regular shoes. Furthermore, our activity recognition model does not require complex sensor fusion algorithms because we use a single IMU on each insole. The computation of activity recognition is executed onboard; therefore, the portable sensing unit can give real-time feedback without requiring a connection to the server or the other devices for the determination. The developed Android application also provides visual feedback and serves as a data logger.
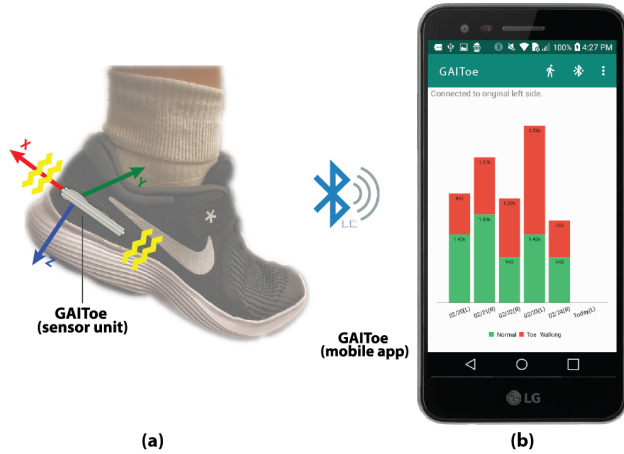
Figure 3.1: Components of GAIToe: (a) a sensor unit mounted on the insole and (b) a linked smartphone application

Our system offers a portable, non-invasive, low-cost, power-efficient, easy-to-use, and quantitative assessment. Our system motivates individuals with ITW to change their walking patterns with continuous remote monitoring in non-clinical settings. Using this system is expected to impact the population with ITW positively.

3.3 GAIToe System Specification

GAIToe is composed of two main components: a shoe sensor unit and a linked smartphone application (Figure 3.2). A sensor unit of the GAIToe, utilizing an IMU, detects toe walking and vibrates onboard. It transmits data to the connected smartphone application via Bluetooth. The sensor unit is designed to measure foot movements using an IMU. It is mounted into an insole to be easily inserted into any pair of running shoes. We programed the sensor unit with a machine learning-based activity recognition for real-time toe walking detection and feedback. The readings of the sensor unit are transmitted to an Android application via Bluetooth. The transmitted data were stored in the cloud-based database. It also displays toe walking and heel-to-toe walking results for the individuals with ITW to review their daily walking patterns.

3.3.1 Hardware Implementation
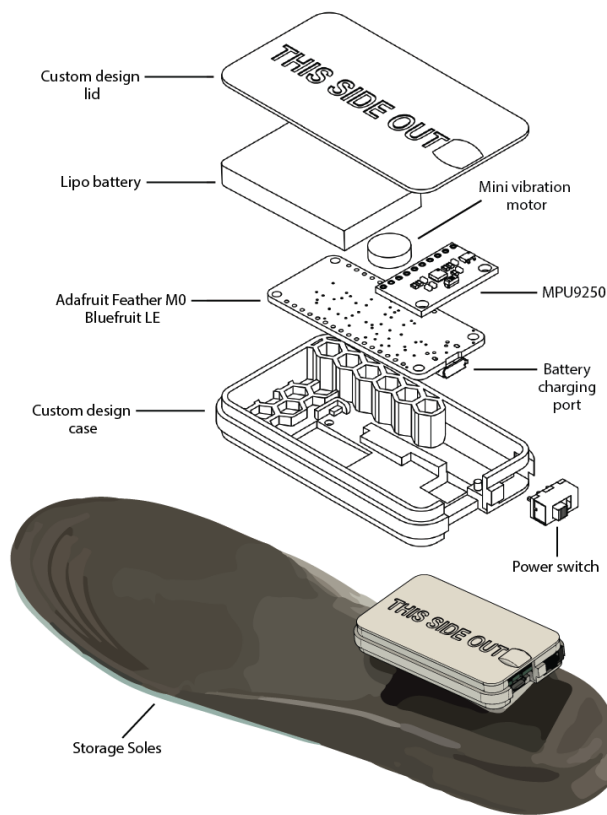
Figure 3.2: Circuit components in the sensor unit

We investigated available wearable sensors, wireless data transmission modules, programmable controllers, and rechargeable batteries with small dimensions to develop remote monitoring and real-time intervention systems for habitual toe walkers in natural settings. Our hardware implementation goal was to maximize the utilization of currently available and affordable devices to reduce the expense of our custom-designed system. The custom-designed 40 mm x 72 mm x 14 mm case is mounted on the storage soles and includes all the circuitry, such as an Adafruit Feather board, an IMU, a mini vibration motor, a Lipo battery, and a slide switch.

With all these considerations, Adafruit Feather M0 Bluefruit LE (Adafruit Industries, New York, NY, adafruit.com) [ada19] development board was chosen. It has an ATSAMD21G18

ARM Cortex M0 processor with up to 48 MHz operating frequency, 32 KB SRAM memory, and 256 KB FLASH. Adafruit Feather provides Bluetooth Low Energy (BLE), low-power, 2.4 GHz spectrum wireless protocol. The Bluefruit LE module (nRF51822) uses the standard Nordic universal asynchronous receiver-transmitter (UART) RX/TX connection profile and enables transmitting data back and forth from an iOS or Android device. Adafruit Feather has a JST connector for a 3.7 V Lithium-Polymer (Lipo) or Lithium-Ion (LiIon) battery. We selected an 800mAh Lipo rechargeable battery as the power supply and connected a slider switch to control it. The built-in micro-USB port on the board allows us to program the microcontroller and automatically switch between USB power and charging the connected Lipo battery at 100 mA. Several indicator LEDs provide the board's status, such as a red LED for power, a blue LED for BLE connection, and a yellow LED for charging. The board's dimension is 51mm x 23mm x 8mm, reasonably small for any wearable device.

GAIToe is equipped with an MPU-9250 motion tracking device (9 degrees of freedom IMU). It is a multi-chip module consisting of a 3-axis accelerometer, a 3-axis gyroscope, and a 3-axis magnetometer (AK8963). The accelerometer has a measurement range of up to $\pm$ 16 g and sensitivity up to $16,384$ LSB/g. The gyroscope has a range of $\pm$ 2000 degrees/sec and sensitivity up to 131 LSB/deg/sec. The magnetometer's full-scale range is $\pm$ 4800 μT, and the sensitivity is 0.6 μT/LSB. Each sensor outputs digitized values through three 16-bit analog-to-digital converters (ADCs). An MPU-9250 communicates with the Adafruit feather board via I^{2}C bus at 400 kHz. The IMU in the insole is located to contact the calcaneus, the heel bone on the hindfoot, as can be seen in Figure 3.1a. It captures the shoe acceleration, angular velocity, and magnetic north.

A mini vibration motor is connected to the Adafruit Feather board to provide real-time biofeedback. When the user is continuously toe walking or consistently standing and sitting on the toe (sitting heel raises), the GAIToe sensor unit produces two types of vibrations: short and long. Following three, six, and nine consecutive toe contacts (walking, standing, or sitting) on the ground, the GAIToe sensor unit generates a 1-second short vibration.

Following ten consecutive toe contacts, it generates a 30-second long vibration. The vibration can be turned off with a heel strike. This vibration generation protocol was defined in consultation with orthopedic surgeons and physical therapists as what would successfully arouse the user's attention regarding toe walking and motivate more heel strikes.

Storage soles [Coo19], insoles with a container space at the bottom, satisfied our need to house the shoe sensor unit and to insert it into any pair of running shoes. Storage soles are made from flexible polyurethane (PU) foam, so they are waterproof and easily trimmed for nearly any shoe size. We designed a case and lid to house the circuitry components and fit them into the storage soles. The container and lid are made by a 3D printer using polylactic acid (PLA), a common plastic filament material. The empty space in the container is filled with hexagons to endure the weight of the human body. The custom-designed 40 mm x 72 mm x 14 mm case includes all the circuitry (Figure 3.2), such as an Adafruit Feather board, an IMU, a mini vibration motor, a lipo battery, and a slide switch.

3.3.2 Power Consumption
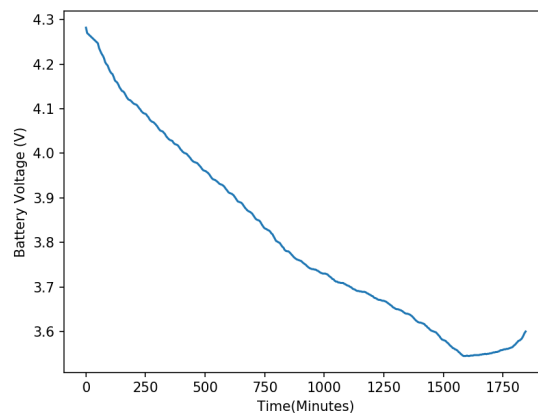
Figure 3.3: Battery characteristics of the sensor unit

The system's power efficiency is crucial for monitoring foot activity and giving continuous real-time intervention. We attempted to emulate a worst-case usage scenario, continuous

toe sitting, including a series of vibrations and a transmission rate at 20 Hz. A typical Lipo battery maintains around 3.7V for much of the battery life, then decreases in voltage just before the circuitry cuts it off. In our experiment, the battery almost consistently discharged the voltage and stayed at the minimum of 3.545V for 30 minutes. Interestingly, the battery increased the voltage up to 3.6V before it turned off (Figure 3.3). We figured out that the system lasts 1,845 minutes (30.75 hours) under continuous operation, as shown in a battery discharge curve in Figure 3.3). Our system fits in clinical settings as well as continuous, pervasive monitoring in naturalistic settings because it requires getting charged once a day.

3.3.3   Android Application Development

Our sensor unit is implemented to compute activity detection on the board but does not have a data logging component. We could add data storage, like an SD card, in the unit, but that would require an extra step of transferring data to monitor daily walking patterns. Due to the recent advancements in mobile technologies, smartphones are commonly used as a communication hub in remote monitoring systems [CLT16, LWZ16, GFE19]. We developed an Android app (Figure 3.1b) to achieve wireless data transmission, collecting data from our sensor unit via Bluetooth, and storing the data in the cloud-based database via the Internet. We focused on a design with minimal user interaction.

The Android application includes a specific Bluetooth connection protocol to automatically connect to the GAIToe sensor unit. When the app is launched, it scans and connects to the BLE module using the pre-stored MAC address. The UART serial communication between the BLE module and the Android device begins when the Bluetooth connection is stable. If the UART service fails within 20 seconds, the app automatically terminates the BLE connection and scans the BLE module again. The Bluetooth connection can be reset manually by pressing the (three-dot) Connect button on the top right corner of the screen (Figure 3.1b). The Bluetooth icon next to the Connect button indicates BLE connection status in four colors: disconnection in red, scanning phase in orange, stable connection with

UART in white, and failed UART service in black. The average time for the Bluetooth connection was 5.242 seconds in an experiment with the LG Phoenix 4 smartphone (which has an Android 7.1.2 Nougat operating system and 1.4GHz Quad-Core Qualcomm Snapdragon processor). The GAIToe sensor unit transmits the IMU's raw signals, the detected activities, and the generated vibration feedback to the connected app with 20 Hz.

The developed app provides an intuitive visualization of the daily walking pattern. Our app calculates an accumulated number of strides based on the received types of activity from the sensor unit. Because our system is deployed to each foot independently, the strides are counted instead of the steps. For instance, the stride length is the distance between two consecutive right foot stances before and after the swing phase during the gait cycle. A stacked bar chart displays the number of toe strides in red bars and the number of heel-to-toe strides in green bars (Figure 3.1b). The stride counts for the previous six days are shown on the first 6 bars, while the real-time stride counts are shown on the rightmost bar. The app saves the collected data into the cloud-based database every five minutes.

3.3.4 Activity Classification Model

The IMU in the insole was sensitive to any foot movements. Based on our experiments, machine learning models enabled us to achieve better activity classification accuracy with the IMU signals instead of a threshold-based classification. We first collected activity data from 14 healthy adults recruited from the university community to generate an activity classification model. The subjects were asked to wear our study shoes, varying from youth's size 6 to women's size 11. Then, they performed 200 strides of heel-toe walking and toe walking, as well as 2 minutes of sitting and standing. We made use of our Android application with an added functionality to save the activity label and the subject ID along with the sensor data in the database.

Feature extraction is an essential step to train a machine learning model. First, the magnitude of the 3-axis of accelerometer, gyroscope, and magnetometer is computed using

Equation 3.1 where i is the index of the signal.

$$A_i = \sqrt{x_i^2 + y_i^2 + z_i^2} \tag{3.1}$$

x_i, y_i, and z_i are the three-axis of vectors. A low-pass filter [Ani19] is applied to each vector of the accelerometer. The roll and pitch angles [Ani19] from the accelerometer is derived. The tilt angle [b22] of each sensor on the IMU is calculated as well. A sliding window approach is also applied to the collected time-series data. Each time-series signal is divided into a non-overlapping window of 10 samples to increase the classification accuracy with various walking paces. Then, the mean and standard deviation of each window are extracted using Equation 3.2 and 3.3.

$$WindowAverage_t = \frac{\sum_{i=1}^{n} x_i}{n} \tag{3.2}$$

Where x_i is a signal reading with index i and n is the size of the window which here is assumed to be 10.

$$WindowStandardDeviation_t = (\frac{\sum_{i=1}^{n}(x_i - WindowAverage_t)^2}{n-1})^{\frac{1}{2}} \tag{3.3}$$

An extra-trees classifier from Scikit-Learn [PVG11] has the highest cross-validation (CV) result with our dataset among other classifiers. The extra-trees classifier fits several randomized decision trees on the subset of the given dataset and then uses averaging to control overfitting [PVG11]. Two hyperparameters of the extra-trees classifier are used to control the learning process: estimators and depth. The number of estimators corresponds to the number of the decision trees, while the depth is the maximum depth of the decision tree in the forest. Figure 3.4 demonstrates the cross-validation scores of examining 1 to 100 estimators and 1 to 20 maximum depths. Because the microcontroller's flash memory or program space is limited, we selected the minimum possible values of the hyperparameters with good

performance. The best 10-fold cross-validation was 88% and was achieved by setting the estimator to 25 and the maximum depth to 8.
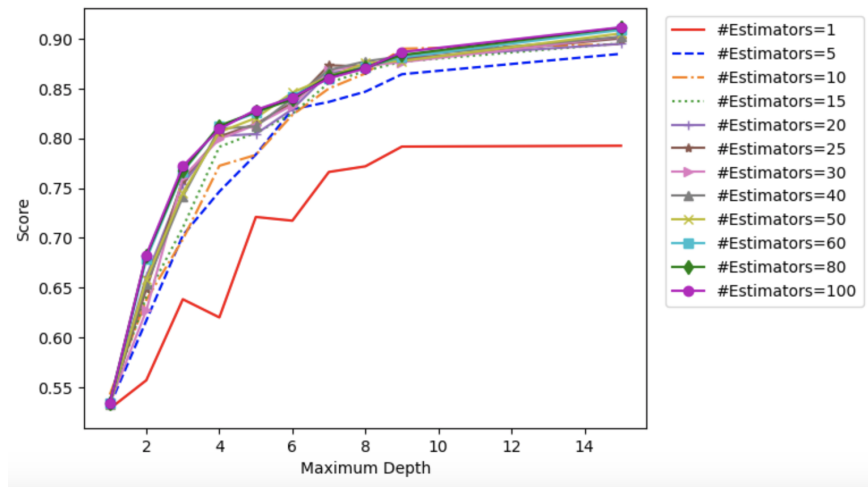
Figure 3.4: Cross validation score of extra-trees classification using a various numbers of estimators and maximum depths.

A tree-based feature selection method [PVG11] removes the irrelevant features on our classification model. The most significant features among the other extracted features include acceleration pitch and tilt angle mean, gyroscope magnitude mean, and standard deviation of gyroscope raw signal values. The activity labels, such as toe walking, normal walking, toe standing/sitting, or normal standing/sitting, are utilized as the classes that we want to predict in the supervised learning. The precision, recall, and F1-score of each class are reported in Figure 3.5. The normal sit/stand class has the highest precision and lowest recall; however, the toe walking class holds the lowest precision and highest recall. All four classes have roughly the same f-1 score.

3.3.5 Stride Counter Algorithm

Comparing the number of strides in toe walking or heel-toe walking is an excellent source to understand the progress of toe walking. As soon as the activity of the windowed samples
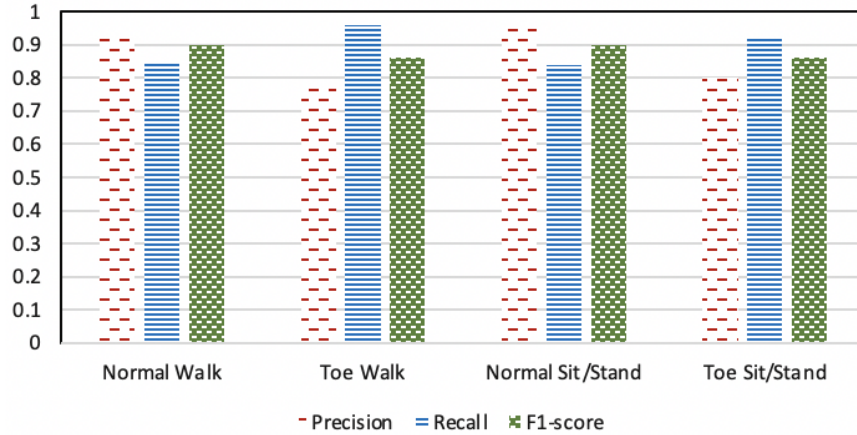
Figure 3.5: Precision, recall, and F1-score of the activity classification model

is determined as toe walking or normal walking with the activity classification model, we need to count the number of strides. Each foot has a swing phase after a stance phase in the gait cycle. The swing phase causes increased signal values in the gyroscope. Therefore, the nonconsecutive peaks on the magnitude of the gyroscope signal correspond to the number of strides. We defined the peaks as the samples above the window average and counted a stride only for the first sample of consecutive peaks.

For example, Figure 3.6 elaborates the stride count procedure in two consecutive windows of the magnitude of the 3-axis gyroscope. The windows are separated by a grey vertical dashed line, while a horizontal dashed line depicts the window average. The peaks, which are higher than the window average, are marked with red triangles. In the first window with ten samples, the 1st, 5th, 6th, 7th, and 9th values are higher than the window average. The sequence of 5th, 6th, and 7th samples are considered as one stride. As an example of handling consecutive windows in Figure 3.6, the last signal (index 9) of the first window and the first signal (index 10) of the second window are both marked as peaks. Since the first window's last signal and the second window's first signal are consecutive, these two consecutive peaks are considered as a stride. So, total five strides were counted within two windows of the gyroscope signal in this example.
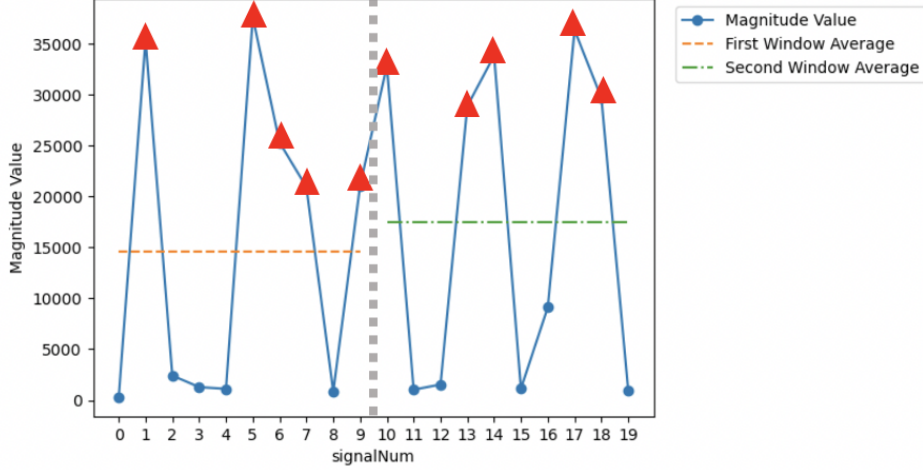
Figure 3.6: Stride counter in two successive windows

As previously explained in the Hardware Implementation section, the GAIToe sensor unit vibrates for detected toe walking, toe standing, or toe sitting. Giving these vibrations can notify the users about their continuous toe strikes and remind them to put their heels down to the ground. The vibration is generated based on the number of consecutive toe strides. Our system also provides intervention for toe standing or toe sitting because orthopedic surgeons and physical therapists suggested that ITW patients are less likely to put their heels down even while standing or sitting. The same vibration generation protocol is applied to the number of toe strikes. If toe standing or sitting persists for 400 milliseconds, it is counted as a toe strike. For instance, a short vibration occurs after 1200 milliseconds of toe standing, corresponding to three toe strikes. A long vibration stops as soon as there is a heel strike, which appears when the detected activity during the vibration period is heel-to-toe walking, normal sitting, or normal standing. We integrated the C-based extra-trees classification model and the stride counter algorithm into the microcontroller.

3.4 Experiments

Ten healthy adults between the ages of 21 and 44 volunteered for the preliminary system validation of GAIToe. They placed the smart insole into their own running shoes and performed six activities: 100 strides of toe walking, 100 strides of normal heel-to-toe walking, 2-minute toe standing, 2-minute normal standing, 2-minute toe sitting, and 2-minute normal sitting. We instructed the participants to perform these activities correctly to obtain clear data. Then, the participants walked at their own comfortable pace on level ground. The sensor recordings and the computation results were transmitted to the connected Android device to be stored.

Figure 3.7 shows the results of our activity detection and stride counter algorithm evaluation. The solid blue bars show the number of correctly detected heel-toe normal strides. There are no incorrectly detected toe strides within normal walking. The green hatched ($//$) bars represent the number of correctly detected ones out of 100 toe strides. Finally, the red dotted bars demonstrate the number of incorrectly detected heel-toe steps through 100 toe strides. The average accuracy of heel-toe stride counts is $93.6\% \pm 3.2$, while the accuracy of toe stride counts is $84.1\% \pm 5$.

To evaluate our vibration protocol performance, we kept a record of the short and long vibration occurrences while the participant walked for 100 toe strides. Table 3.1 presents the number of short and long vibrations within correctly detected toe strides. It also includes the expected number of short and long vibrations on the last two rows. Any incorrectly detected heel-toe strides or a heel strike during the 100 toe stride measurement disrupt the vibration generation based on our protocol. The mean absolute error (MAE) is 0.7 for short vibration and 0.3 for long vibration.
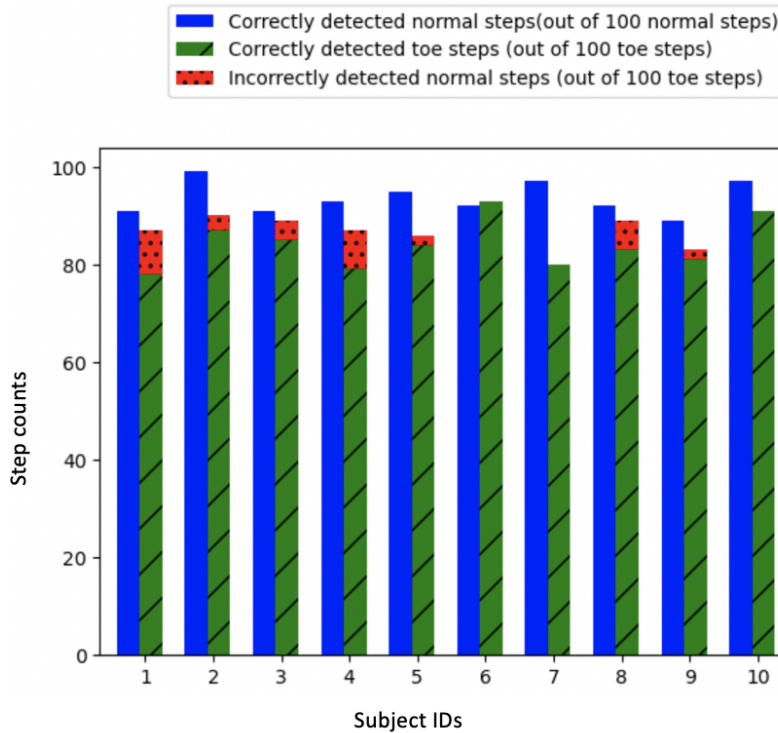
Figure 3.7: Number of strides detected per subject.

3.5 Future Work

The repeated usage and pressure on the insole can break our custom-built sensor unit because it is located underneath the hindfoot, a place within the foot region that holds high-pressure values [MSC19]. Since the IMU is sensitive to any small movements of the foot, we need to enhance our detection algorithm to reduce possible false positives by applying various signal processing or machine learning techniques. In addition, our system can be extended to identify gait parameters of the entire population, which is reliable in different situations, such as taking the stairs or walking on an uphill path.

After the system validation of the GAIToe, we finally 3D-modeled and customized the different sizes of insoles implanting all electronic components, as shown in Figure 3.8. Also, 3D printing with a flexible material achieved better system durability and performance. The

Table 3.1: Number of short and long vibration occurrences within 100 toe strides per subject

Subject ID	1	2	3	4	5	6	7	8	9	10
Correctly detected toe steps	78	87	85	79	84	93	80	83	81	91
Short vibrations	20	27	26	23	25	28	24	25	24	28
Long vibrations	6	8	7	6	8	9	8	8	8	9
Expected short vibrations	23	26	25	24	25	28	24	25	24	27
Expected long vibrations	7	8	8	7	8	9	8	8	8	9
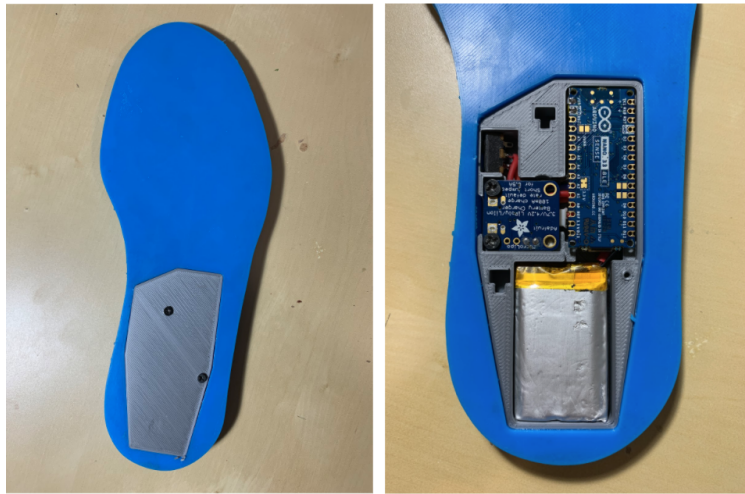
Figure 3.8: Finalized version of the smart insole is 3D printed entirely and embeds all electronic components
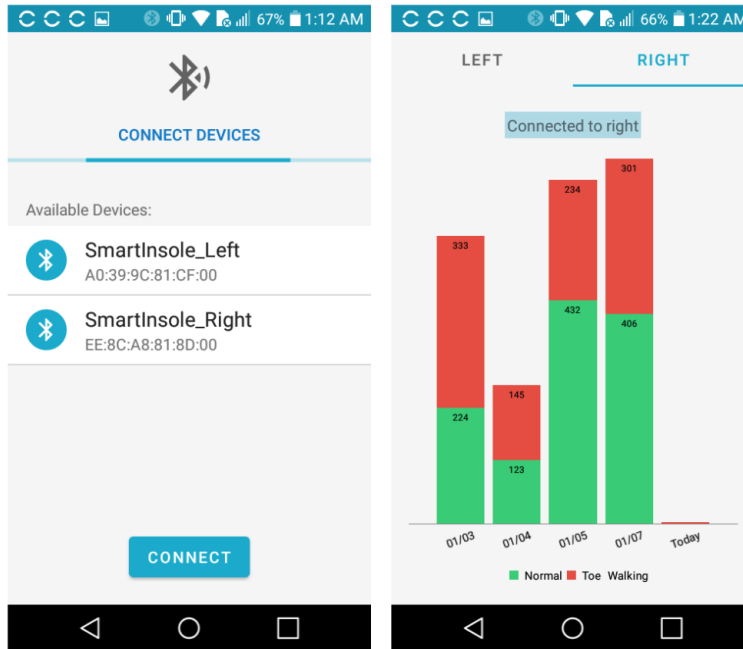
Figure 3.9: Finalized version of the Android app

Android application is also updated to have a more stable BLE connection (Figure 3.9). We have recruited children with ITW through the local children's hospital. We provided Nike Revolution 5 FlyEase running shoes to the study participants as a constant measurement instrument. These running shoes have a wraparound zipper that is convenient for inserting and removing our insoles. The subjects and their parents were educated to alter the insole based on their shoe size and install our software on a study Android device to monitor subjects' daily toe and heel-toe steps. We asked the study participants to run our Android app in the background and wear the waist bag with the smartphone while trying our shoes. They were responsible for charging the system every day. Finally, we gave the final version of the smart insole to 14 children with ITW and completed data collection. About half of the subjects remarkably reduced toe walking percentage after using our smart insoles. This result proves that our gait monitoring system benefits ITW patients with real-time feedback. The effectiveness and robustness of our system are validated. We are still actively analyzing the data to find features affecting the children's walking behavior.

3.6　Conclusion

This chapter proposed GAIToe, a remote-monitoring system for activity recognition and improving walking patterns of individuals with habitual toe walking. GAIToe provides a wearable, portable, energy-efficient, and low-cost platform for pervasively monitoring walking patterns in daily life. Our sensor unit, utilizing an IMU, is designed to be inserted into any pair of running shoes. The proposed machine learning-based activity classification model identifies different activities on the device, not utilizing cloud computing. The stride counter algorithm identifies the number of strides with high accuracy and gives real-time biofeedback. The system has been validated through an experiment on ten healthy subjects. In addition, the connected Android app provides data visualization regarding walking patterns.

GAIToe may enable orthopedic experts and researchers to investigate the detailed gait parameters and foot movements of ITW in natural settings. Furthermore, healthcare professionals can monitor the patients' progress remotely. It may become an assistive tool to develop a more effective intervention technique to improve an individual's walking behavior.

CHAPTER 4

Remote Exercise Tracking For Knee Rehabilitation

4.1 Objectives

Knee reconstructive surgery, like ACL (Anterior Cruciate Ligament), is one of the most common orthopedic procedures in the United States. Proper rehabilitation is important for recovery from a knee reconstruction and replacement surgery. Patients are likely to experience pain and stiffness, extension issues, and delayed strength recovery without it. Most rehabilitation programs include a set of exercises to improve the knee's range of motion, weight-bearing capacity, and overall strength [SN90]. However, current orthopedic treatments and rehabilitation exercises mainly do not support quantitative measures of knee movements or provide real-time biofeedback. Additionally, visiting orthopedists and physical therapists costs a lot of time and money that many patients cannot afford. To overcome these challenges, an intelligent way of tracking the patients' rehabilitation progress needs to be developed.

This chapter introduces a remote exercise tracking system for knee rehabilitation. Our system measures the knee flexion-extension angle using an embedded flex sensor in a commercial hinged knee brace. The connected Android application receives and transmits the sensor values to the cloud-based database. Real-time monitoring of knee movements improves the quality of therapeutic exercises and knee rehabilitation.
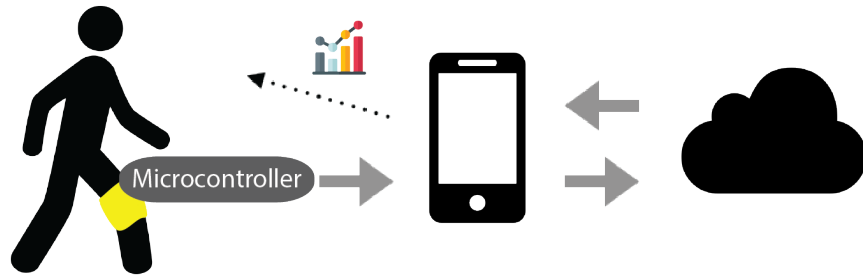
Figure 4.1: EXTRA system architecture.

4.2 Related Works

Several studies have proposed utilizing body sensor technologies to monitor physical activities on the knee joint and proved their positive effect on knee health [LKB98, PKK01]. In [SMA87], electromyographic (EMG) analysis was used to compare the therapeutic effects of different knee exercises. This study showed that different types of knee exercises lead to different levels of muscle activation, influencing the overall therapeutic effect as well. In [MIH13], gyroscope and flex sensors have been suggested for measuring the knee joint angle. However, simply attaching the flex sensors underneath the knee with the elastic supportive cloth caused the sensor to easily break while bending. In [QSG13], the knee angle was measured using the Ultra-Wide Band (UWB) transceivers. This study measured the knee angle by setting two antennas on the adjacent part of the knee joint and a Time of Arrival (TOA) estimator to calculate the distance between these two antennas and the knee angle using the law of cosines. However, these proposed devices were difficult to deploy and did not support portability and mobility. In addition, their measurements are mostly recommended to be completed in an indoor setting. We have focused on developing a portable, affordable, low power consumption, easy-to-use, and real-time monitoring system for therapeutic knee exercises.

Figure 4.2: Flex sensor on the metal hinge (left) and knee brace embedding the flex sensor (right).

4.3 EXTRA System Specification

We introduce **EX**ercise **TR**acking and **A**nalysis (EXTRA) platform, a remote monitoring system of knee movement (Figure 4.1). EXTRA has three main components: data acquisition, mobile application, and data storage.

4.3.1 Data Acquisition

The data acquisition component monitors the knee movements using a smart knee pad and transmits the time-series sensor readings to the connected Android device. We have developed a smart knee pad by embedding a 4.5-inch flex sensor on a commercially available knee brace (Figure 4.2). One end of the flex sensor was affixed on a metal hinge of the knee brace, and the sensor has covered the circuit with fabric. The resistivity of the flex sensor

or the voltage difference on the two ends changes based on the degree of bending.

The flex sensor is connected to a microcontroller for operation and data transmission. Adafruit Feather [ada19], a light, affordable, and Arduino compatible microcontroller board, is well-designed to be equipped on wearable devices. The Feather board has a JST jack to connect with a 4.2/3.7V Lithium-Polymer (Lipo/Lipoly) or Lithium-Ion (LiIon). An 800 mAh Lipo battery was connected to power the board. The built-in USB port allows us to program the microcontroller and recharge the connected battery at 100mA. An LED on the board starts blinking while the power is on. We manually added a power push-button to minimize the power consumption and make it more convenient for the users to power on/off the board. The Feather board also includes a Bluetooth Low Energy (BLE) capability, which is a low-power and 2.4GHz spectrum wireless protocol.

4.3.2 Mobile Application

A connected Android application converts the sensor readings from the knee pad to the angle of flexion and extension in degrees. We observed that the sensor readings and the linear motion of the knee joint are linearly correlated. For the sensor reading calibration, we used a linear interpolation (4.1) where (x_1, y_1) and (x_2, y_2) are two different angle observations. The app uses (4.2) to convert the received sensor readings (s) to the knee joint angle (A).

$$b = y_1 + (x - x_1)\frac{y_2 - y_1}{x_2 - x_1} \tag{4.1}$$

$$A = s \times x + b \tag{4.2}$$

The Android application also has data receiving and transmitting capabilities to link the smart knee pad and the cloud-based data storage. The mobile app collects sensor signals via Bluetooth and sends and saves the data to the database via the Internet. A BLE connection protocol on the app links the smart knee pad without the user's extra input. As soon as

Figure 4.3: Android application of EXTRA: a real-time monitor of the knee joint angle (left) and an exercise progress chart (right)

the smart knee pad is on and the app launches, the app automatically searches the BLE module on the Feather board by the unique MAC address. The app also transmits the sensor recordings and processed data, such as knee joint angles and the maximum angle during the knee movement, to the cloud server for storage purposes only, not processing purposes.

Furthermore, our user-friendly mobile application provides a real-time monitor of the knee flexion and a daily summary of the activities. The left screenshot of the figure 4.3 shows the charts of the knee joint angle, and the right screenshot shows the knee activity progress chart. The users can easily understand the connection status with the knee brace. The users can also catch the flexion angles during the knee exercise through the numerical value and the illustration. The exercise progress chart shows the daily achievement of exercise duration in green and the maximum knee angle in blue. The exercise duration increases when active knee movements are detected using the standard deviation. The *Beat Your Record* line indicates the maximum angle that the user reached through the exercise and encourages the user to achieve a better performance than their records.

Table 4.1: Mean absolute error of measured knee angles

Angle	MAE
0	0.19
15	8.74
30	24.95
45	12.13
60	15.06
75	13.07
90	17.68
105	14.66

4.4 Experiments

The accuracy of the knee angle measurement and the system usability were evaluated by eight healthy adults (3 female, 5 male, age range: 23-27). We asked the participants to wear the knee brace and bend their knee in different angles while sitting down on a chair. Each participant measured a knee angle from 0.0 to 105.0 degrees with increments of 15.0 degrees for 30 seconds each. The participant also performed two exercises: sitting quad lift and standing knee lift. These exercises allowed them to experience the mobile app's interface with knee movement by wearing the knee brace. At the end of the experiment, the participant filled out a questionnaire regarding the usability of our system. The questionnaire was developed based on the Usefulness, Satisfaction, and Ease of use (USE) questionnaires on [Lew95] and [Lun01].

4.5 Results

Table 4.1 shows mean absolute error (MAE) for each angle measurement. The average MAE was 13.31 degrees, and this value indicates sufficient accuracy for monitoring therapeutic exercises. Our knee joint angle measurement system is quite sensitive about the body postures and different shapes of the leg. We observed that bending the spine or moving the arms caused changes in the measurement of the knee joint angle. A participant with lateral pelvic tilt had a higher MAE about the angle measurement than others. Further calibration is required to support reliable knee flexion-extension angle measurement.

The results of the usability questionnaire are shown in table 4.2. The average score of 9.6± 0.42 of the questionnaire results indicates that our system has high usability and effectively delivers information about knee activity. The mobile app does not require complicated instructions, and any individual can easily install and interact EXTRA platform easily.
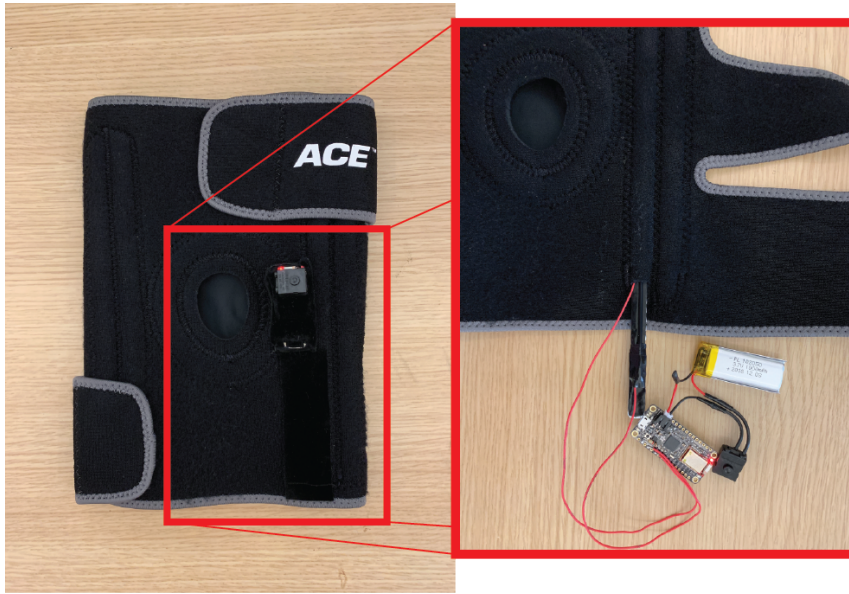
Figure 4.4: Updated version of EXTRA implanting a conductive rubber stretch sensor

4.6 Upgraded Version of EXTRA

Our initial design used a 4.5-inch flex sensor, which changes the resistivity by deflection or bending. However, the vulnerability of the flex sensor was not suitable for repeated usage inside the knee brace. Therefore, we have developed a smart knee pad by embedding a 4-inch long conductive rubber cord stretch sensor [Ind] on a commercial knee brace with a supportive metal coil. A low-cost stretch sensor is made of carbon-black impregnated rubber and increases the resistivity as it is stretched up to 50 to 70% of the resting length. The resistance is about 350 ohms per one inch long. It is not fragile like a flex sensor. However, one drawback of using the rubber-based stretch sensor is that the sensor values may not always be precise because the pulled and released rubber takes a minute or two to return to its original length or resistance [Ind]. Therefore, sensor calibration using linear interpolation (4.1) is required at the beginning of using the system to increase the precision of the measurement of the rubber stretch sensor. Conversion from the sensor recordings to the knee angle in degrees is completed using 4.2 as well.
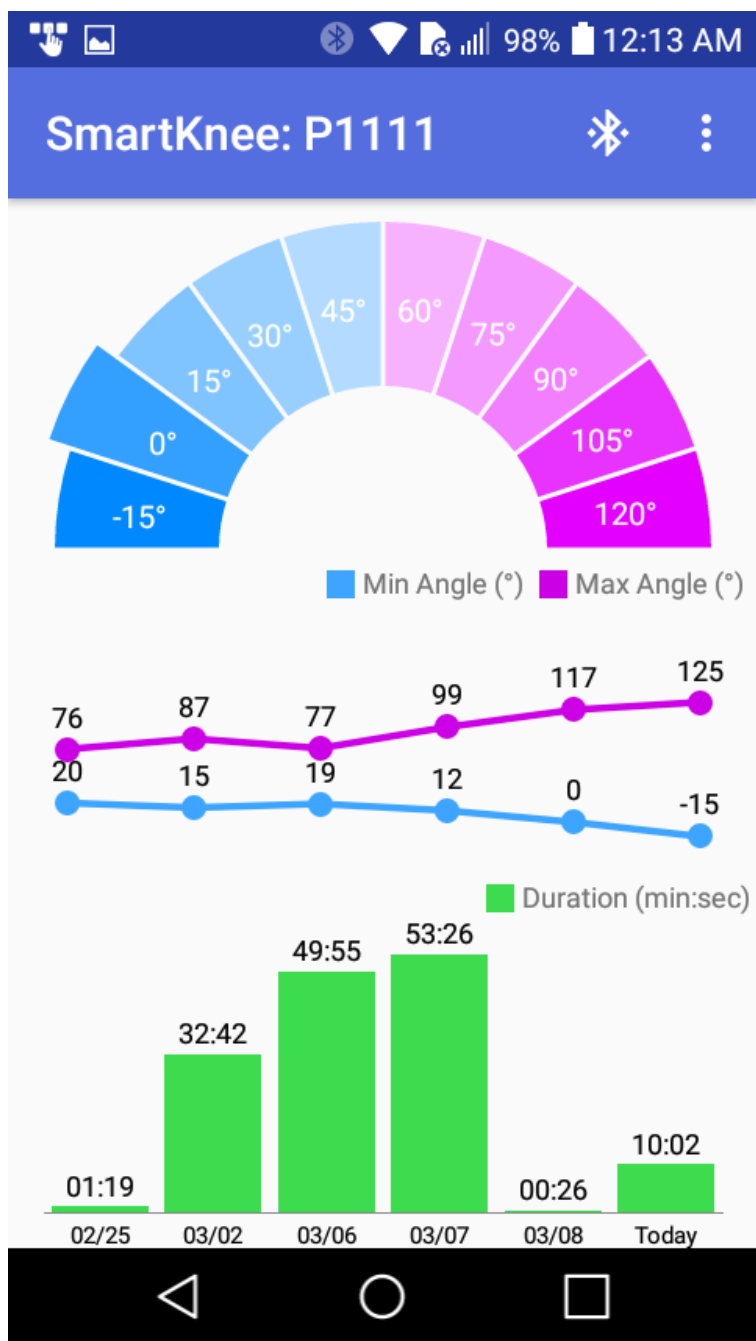
Figure 4.5: *SmartKnee for patients*: knee exercise tracking app for the patients.
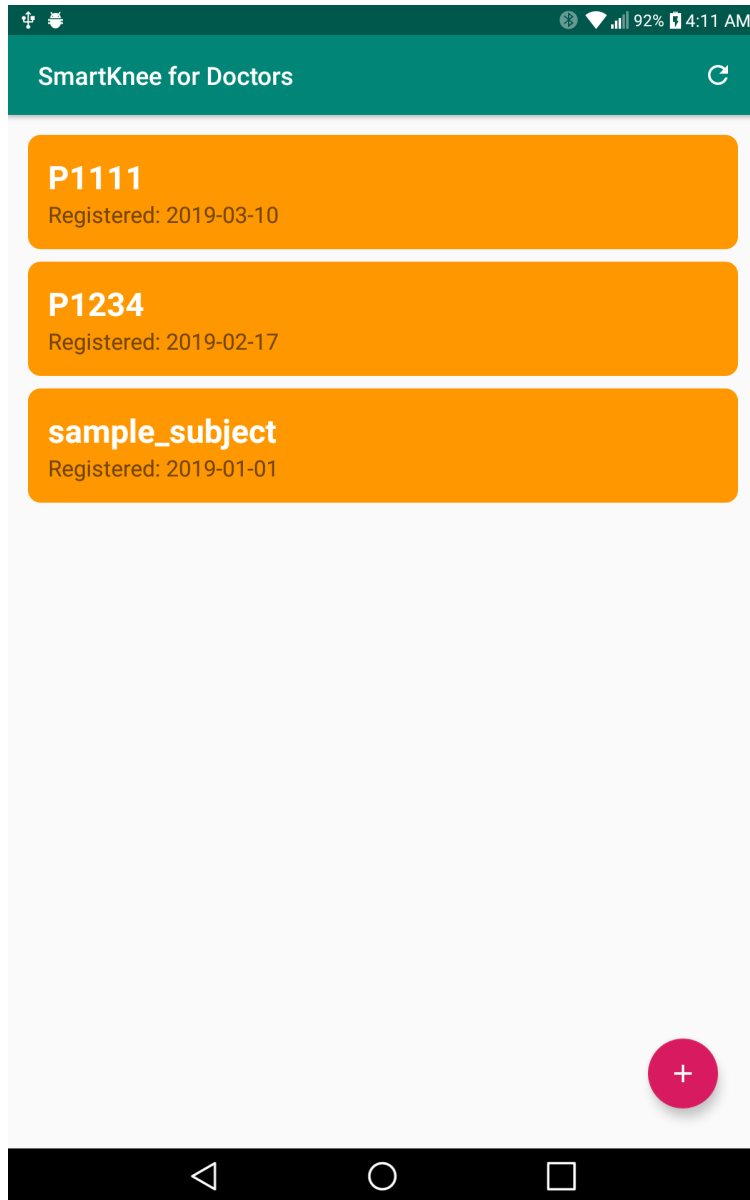
Figure 4.6: *SmartKnee for doctors*: patient-list page on the dashboard app for the doctors.
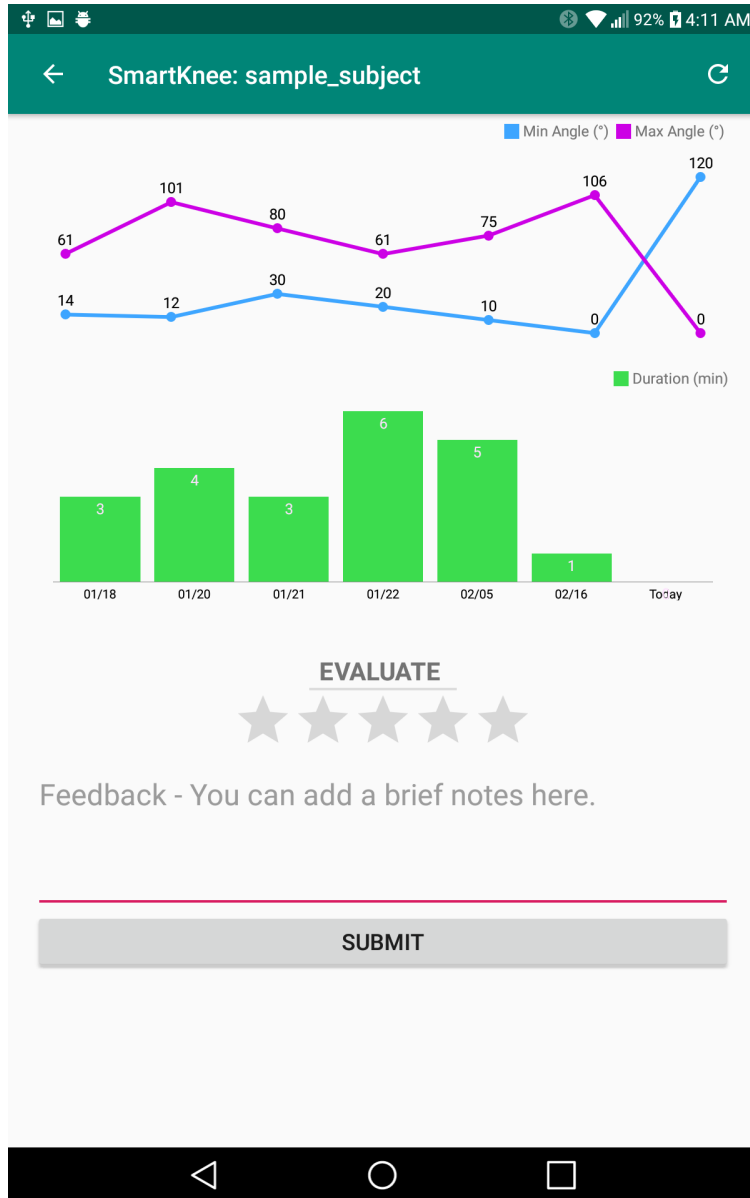
Figure 4.7: *SmartKnee for doctors*: patient-specific page on the dashboard app for the doctors.

For the updated version, we developed two different Android apps for different users: *SmartKnee for patients* and *SmartKnee for doctors*. The *SmartKnee for patients* (Figure 4.5) provides real-time knee exercise tracking based on the usage of the smart knee pad. The real-time flexion angles during the knee exercise are shown on the half-circle chart. The progress charts include the line charts in the middle and the bar chart at the bottom of the screen. The line charts represent the maximum and minimum angles that the user could reach. The bar chart displays the exercise duration in minutes and seconds. The exercise duration does not elapse if there is no knee movement for 10 seconds. The progress charts show the real-time changes on the rightmost as well as daily maximum and minimum knee angle and the exercise duration of the past six days. The BLE connection status is noticeable by the Bluetooth icon on the right top corner. This compact interface is designed to encourage the user to perform the required exercises better than the previous days.

The *SmartKnee for doctors* is a dashboard app that orthopedic doctors or physical therapists can use to monitor the rehabilitation progress of the registered patients. This app (Figure 4.6) allows healthcare providers to register the smart knee pad of a patient and manage multiple patients in one place. Moreover, the patient-spec page (Figure 4.7) presents the patient's daily knee activity progress. It also provides a function to leave an evaluation about the patient's progress in the form of star rating and comments. Therefore, healthcare professionals may provide optimal and effective treatments for patients.

4.7   Conclusion

We presented EXTRA, a remote-monitoring system supporting exercise tracking and knee rehabilitation feedback. In this chapter, we validated the angle measurement and usability of EXTRA. The updated version EXTRA overcomes limitations on the original version of EXTRA and provides better Quality of Service (QoS). Our system offers a completely wireless, portable, wearable, low-cost, easy-to-use, user-friendly, reliable measure of knee movements.

Recording the progress of knee activity encourages users to do therapeutic exercises for knee-injured patients effectively. EXTRA may benefit both orthopedic professionals and patients to speed up rehabilitation after a knee reconstruction and replacement surgery.

Table 4.2: Usability questionnaire and the average score: participants scored between 1 (strongly disagree) to 10 (strongly agree) to respond each question.

Question	AVG
I am comfortable with using this system again.	9.89
The system provided me with helpful information regarding my knee movements.	9.78
The app was responsive and showed the values in a real-time manner.	8.56
I could effectively perform the requested exercises using the system.	9.67
The knee pad was very comfortable to wear and did not affect the quality of my motions.	8.89
It was simple to learn to use the application (UI).	10.0
Proper messages in the application were provided to inform me of any unexpected behavior.	9.0
I believe this system provides the user with incentives for improving the knee exercises and staying on track.	9.67
I believe that using this system will positively influence the quality of therapeutic knee exercises.	9.89
The visualizations and the information provided by the app were very clear.	9.89
The interface of this system was pleasant.	9.89
The system has all the capabilities I expected it to have.	9.67
Switching the system on and off was easy for me to do.	10.0
It requires the fewest steps possible to accomplish what I want to do with it.	9.89
I was able to use the system without written instruction.	9.33
I did not notice any inconsistencies as I use it.	9.0
Setting up the system for an exercise session, including wearing the knee pad and starting the app was very simple.	9.33
I easily remember the steps of using this system.	10.0
I would recommend this system to others.	10.0
Overall, I am satisfied with using the system.	9.67

CHAPTER 5

Identification of Cognitive Impairment of Elderly

5.1 Objectives

Alzheimer's is becoming a more common cause of death in the U.S. as the population ages. Early detection of mild cognitive impairments (MCI), the stage between normal age-related cognitive decline and the decline from dementia, can help provide optimal care for Alzheimer's patients. Unfortunately, there is no single test to determine the presence of dementia. A diagnosis cannot be completed in one clinic visit because the changes in cognitive function must be observed over time.

Developing a clinical assistive tool using wearable devices to identify MCI can reduce the burden of complex assessment and can be effectively deployed in the patients' daily lives as a form of remote cognitive health monitoring. Recently available wearable devices can measure physiological signs and physical activities. We focused on designing a platform that measures Photoplethysmography (PPG) and gaits in clinical settings.

Photoplethysmography (PPG) sensors are commonly used in commercial and medical heart activity monitoring devices. PPG is an optical technique to measure changes in the blood volume in the blood vessel [SJS08]. PPG signals are acquired by the absorption of red and infrared wavelengths that pass through the fingertip or the earlobe [RMK12]. PPG also has the potential to measure cognitive function using heart rate variability (HRV), which is the beat-to-beat variations in heart rate. HRV is strongly related to the individual's cognitive function, including memory performance, attention, and executive function. According to a

study by Hansen et al. (2003), the higher HRV group has a better performance of higher correct responses and faster reaction times on working memory and continuous performance tests [HJT03]. A study by Duschek et al. (2009) investigated that on-task peak-to-peak interval and the power of the mid-frequency band of HRV are negatively correlated with the individual's attentional function [DMW09]. Taelman et al. (2009) demonstrated that mental task changes the heart rate and HRV [TVS09]. Shah et al. (2011) had a study that controlled familial and genetic influences and found statistically positive associations between HRV with verbal memory and a learning task [SSV11].

Gait abnormalities are associated with the early stages of cognitive decline. Gait requires multiple cognitive inputs to maintain an upright posture and motor control and to shift and avoid obstacles [DMH14]. The study of Verghese et al. (2007) demonstrated that quantitative gait parameters, such as pace, rhythm, and variability, predict the risk of cognitive decline and dementia [VWL07]. Mielke et al. (2012) also investigated that relatively faster gait speed is associated with better memory performance and executive function [MRS13]. They used a timer and a mat with embedded presser sensors to measure quantitative gait. However, our assessment system uses the accelerometer and gyroscope sensors on a smartwatch that offers gait qualities and an easier installation.

In machine learning techniques, feature extraction is essential to get useful information from signals, but feature selection is also significant for successful classification. Several studies [PPL12, SBK07, LM11] indicate that extracted features from bio-signals are redundant. Several feature selection methods for the bio-signal classification are found in different research studies. A study by Kavsaoglu et al. demonstrates a feature ranking algorithm for successful biometric identification using PPG [KPB14]. A feature ranking algorithm has simplicity and scalability but still needs a search algorithm to find the best subset of features. For electroencephalography (EEG) signal classification, the genetic algorithm has been used to search the space of feature subsets [KPB14, SBK07]. The genetic algorithm works well for heuristic local search and optimization; however, it is computationally time-consuming.

Figure 5.1: System architecture for bio-signal assessment.

Table 5.1: Demographic summary of study participants

Variable	Total (n=69)	PPG (n = 63)	Gait (n = 53)
Age, years	72.45 ± 10.55	72.76 ± 10.55	71.58 ± 11.36
Male, %	49.28	49.21	47.18
Education, years	17.06 ± 2.25	17.00 ± 2.23	16.94 ± 2.33
Right-handed, %	86.96	85.71	88.68
MCI diagnosis, %	49.28	50.79	50.94

The sequential Floating Forward Search (SFFS) algorithm has been used for electrocardiography (ECG) signal classification [LM11]. SFFS is an exponential cost algorithm and sequentially adds or removes features (like floating around) until finding the subset with the best evaluation [MBN].

5.1.1 Neuropsychological Assessment

We applied our system to 69 participants in a longitudinal aging study at the UCLA Easton Center for Alzheimer's Disease Research. We collected PPG signals during three neu-

ropsychological tests: California Verbal Learning Test-II (CVLT-II), Auditory Consonant Trigrams (ACT), and Stroop. We selected these three tests as mental stressors because they assess memory, attention, and executive skills, respectively, which can be affected by the disease. Besides, since participants may have difficulties with these tests, we planned to determine if these were associated with physiological changes.

Diagnoses were defined through consensus conferences that included neuropsychologists and physicians. Exclusion criteria included non-degenerative and non-vascular causes of cognitive impairment, unstable medical conditions (e.g., organ failure), and major psychiatric disorders (e.g., schizophrenia). Participants received neurological and neuropsychological evaluations. Diagnoses were made using the National Institute of Neurologic and Communicative Disorders and Stroke and Related Disorders Association (NINCDS-ADRDA) criteria for Alzheimer's disease [MDF84] and the Petersen [Pet04] criteria for MCI. A diagnosis of MCI was given when there was cognitive impairment (i.e., at least 1.5 standard deviations (SD) below the age and/or education-adjusted norms) on at least one neuropsychological measure in a comprehensive test battery, in the context of generally intact activities of daily living. All controls scored above 1.5 SD on their age and/or education-adjusted norms on the neuropsychological measures. The entire data assessment was observed and controlled by researchers in the lab. Diagnosis of cognitive impairment became a label of supervised classification. We divided the subject data into two groups: MCI and cognitively healthy controls for binary classification. The MCI group included all types of MCI, such as amnestic and non-amnestic.

5.1.2 Bio-signal Assessment

Our bio-signal assessment system (Figure 5.1) uses a smartphone as a network hub to collect data from wireless devices and to transmit the data to the database. We developed an Android app to receive physiological signals from Nonin Wireless Finger Pulse Oximeter (Nonin Onyx II 9550; Nonin Medical, Plymouth, MN) [Non] via Bluetooth with a 75 Hz
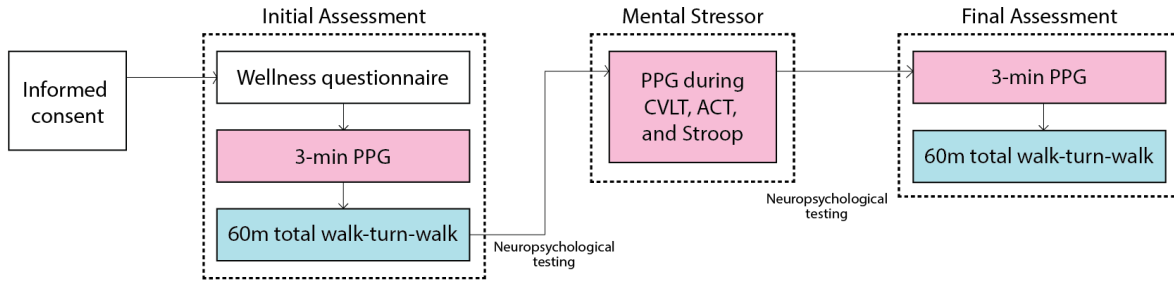
Figure 5.2: Data assessment protocol during the neuropsychological visit.

sample rate and three-axial accelerometer and gyroscope signals from a Samsung Smartwatch (Samsung Gear Live; Samsung Electronics, Suwon, South Korea). Nonin pulse oximeter takes several physiological data: heart rate in beats per minute (BPM), peripheral capillary oxygen saturation (SpO2), and PPG. The Android Wear API was used to deliver the gait assessment from a Samsung Smartwatch. Both wearable devices used Bluetooth with a secure pairing code to connect to the app. The Android app transferred collected data to a Health Insurance Portability and Accountability Act (HIPAA) secure cloud server via Wi-Fi. Our assessment system offers mobility, usability, non-invasiveness, and reliable data transmission, which can be applied to a clinical or home care setting to check cognitive impairment.

Figure 5.2 shows the overall bio-signal assessment protocol. Each participant first completed informed consent and a wellness questionnaire, which has a scale of five. The wellness questionnaire has five criteria: fatigue, mood, stress level, sleep quality, and sleep duration of the day before in hours and minutes. These criteria were modified from the wellness questionnaire for athletes, which was created by McLean et al. (2010) [MCK10].

For the initial assessment, the participant sat still and wore the fingertip pulse oximeter on the index finger of their non-dominant hand to collect a 3-minute PPG. Talking or moving around during the measurement was not allowed to reduce possible artifacts on the signal. The pulse oximeter was taken off after the measurement. The Samsung smartwatch was placed on the participant's non-dominant wrist, and the participant performed the 60-meter total walk-turn-walk activity. The smartwatch was taken off after the measurement. After
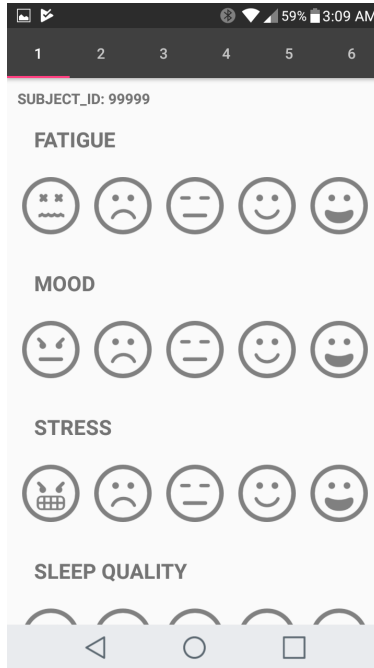
Figure 5.3: Screenshot of Wellness Questionnaire

the initial assessment, the participant had numerous neuropsychological tests. The PPG signals were obtained again during the CVLT-II, ACT, and Stroop tests, which took about 30 minutes. The participant was allowed to talk but was restricted from large hand gestures during the measurement. The final bio-signal assessment was collected again with the same procedure as the initial one.

5.2 Feature Extraction

5.2.1 Gait Variable

The Butterworth filter cleaned noise and restored missing values due to irregular sample delays of accelerometer and gyroscope signals (Figure 5.6). The Butterworth filter is designed to have a flat frequency response in the passband, while the frequency response amplitude of the filter rolls off toward zero in the stopband [HBH16]. Our assessment system simultane-
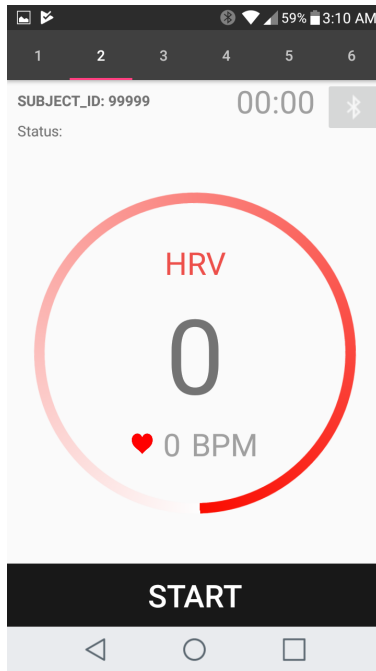
Figure 5.4: Screenshot of PPG collection
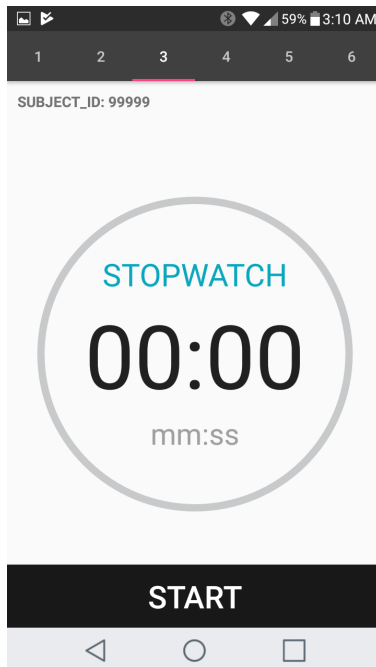
Figure 5.5: Screenshot to gait collection
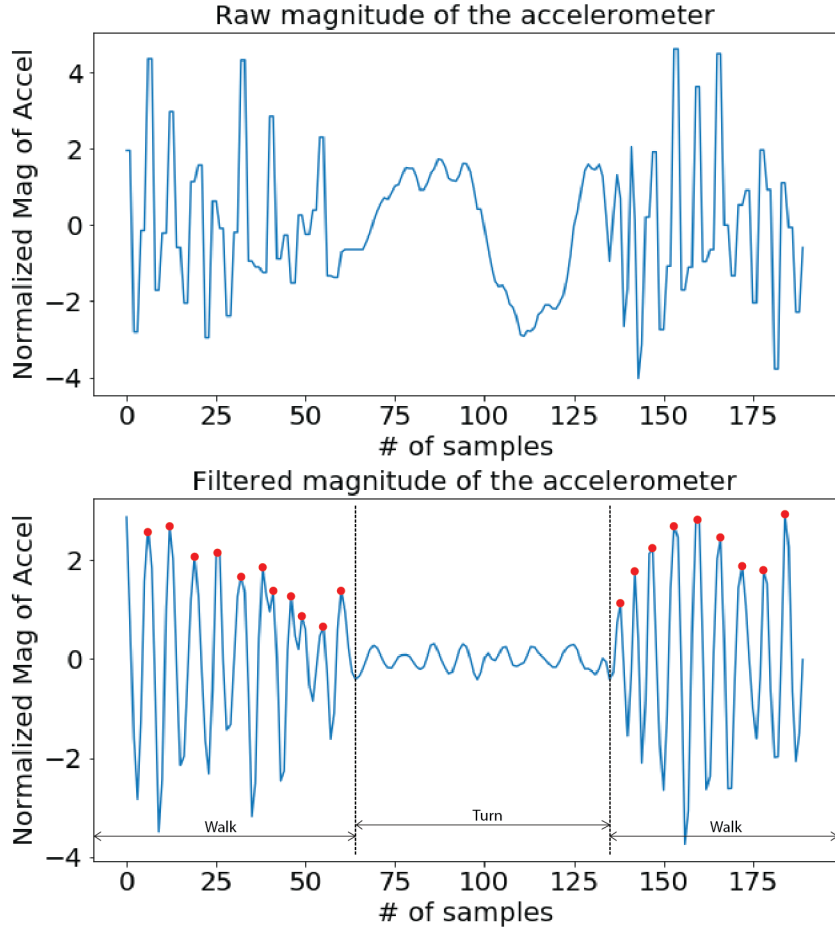
Figure 5.6: Magnitude of the accelerometer signal: a noisy raw signal (top) and a signal after Butterworth filter (bottom).

ously collected accelerometer and gyroscope sensor values through an Android smartwatch. It recorded one timestamp for the two sensor values and caused occasional delays from 5 to 2,145 milliseconds. We averaged different sampling delay (d) and obtained the sampling rate frequency (f_s) using Equation 5.1 [BR15a].

$$f_s = \frac{1}{N} \sum_{i=0}^{N} \frac{1}{d_i \times 10^{-3}} \tag{5.1}$$

The N is the number of samples per measured signal. One-tenth and one-fourth of the sampling rate frequencies were used to set the cut-off of low pass and high pass of the

filter, respectively. Because of several long delays, a signal before using the filter has mostly flat peaks and some steps. However, a filtered signal is smoother, as shown in Figure 5.6. Consecutive walking waves are missing in the middle of each signal assessment because it is a turning point during the walk-turn-walk activity. The Butterworth filter refines signal peaks and flattens noise during the turn.

Peaks on signals are significant points to characterize the gaits. The magnitude of the accelerometer signal was calculated by Equation 5.2 and used to reduce the sensitivity of three-axial smartwatch rotation [UHG17].

$$M_i = \sqrt{x_i{}^2 + y_i{}^2 + z_i{}^2} \tag{5.2}$$

The x, y, and z represent each orthogonal axis, and i corresponds to time. A peak detection algorithm was applied to detect the peaks of each signal correctly. Both accelerometer and gyroscope signals are periodic due to continuous walking activity. We expected to have an equal distance between peaks for each signal. We found a peak detection with minimum peak height (MPH) as 0.4 and minimum peak distance (MPD) as 2 samples perform well on the accelerometer and gyroscope signals.

Gait variables were derived using peaks of the magnitude signals. The number of peaks on the magnitude of the accelerometer (Figure 5.6) reflects a step count. The walking duration was obtained from the time difference between the last and first steps. The average gait speed was calculated by dividing the walking distance by the walking duration, resulting in meters per second. The average step time was considered the average time distance between the accelerometer magnitude peaks.

5.2.2 PPG Variables

PPG variables were extracted from the time-domain and the frequency-domain of PPG signals. We first calibrated each PPG signal by removing the linear trend of time-series.
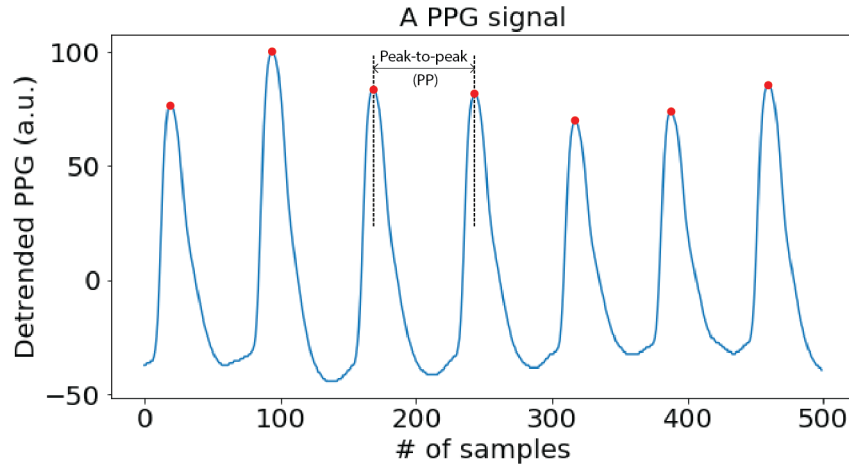
Figure 5.7: An example of PPG signal with the peak detection.

Then, we followed guidelines for the HRV from the Task Force of The European Society of Cardiology and The North American Society of Pacing and Electrophysiology (1996) [Ele96]. The task force provides HRV analysis using ECG, but we applied the same guidelines to the PPG since ECG and PPG are highly correlated. Several studies have proved that peaks of PPG coincide with the R peaks of ECG [SJS08, MRS01]. The R peak is the highest amplitude on a typical ECG and essential for HRV analysis.

A peak detection algorithm was used to extract features from the time-domain of the PPG signal. We expected to have an equal distance between peaks for each signal because PPG is periodic due to continuous heart activity. We found a peak detection with 10 minimum peak height (MPH) and 30 samples of minimum peak distance (MPD) performed correctly on the PPG signals. We calculated the mean (MeanPP) and standard deviation (SDPP) of the peak-to-peak (PP) intervals (Figure 5.7) for three different states: initial, mental stress, and final (Figure 5.2). The square root of the mean squared differences of successive intervals (RMSSD) was also computed using Equation 5.3, which is commonly used as a significant metric of HRV. We also calculated the RMSSD and MeanPP differences between each state, representing the autonomic nervous system (ANS) reaction to the mental stressor. We obtained the average heart rate for each state from the time series of heart rate values.

68

$$RMSSD = \sqrt{\frac{1}{N} \sum_{i=0}^{N} (PP_{i+1} - PP_i)^2} \qquad (5.3)$$

Fast Fourier transform (FFT) was used to extract features from the frequency domain of PPG signals. The power spectrum was divided into three frequency bands: very low frequency (VLF; ≤ 0.04 Hz); low frequency (LF; 0.04 to 0.15 Hz); and high frequency (HF; 0.15 to 0.4 Hz) [Ele96]. The power of each frequency band became a distinct feature. The distribution of power of LF and HF may vary due to the modulations by the ANS [Ele96]. Thus, we calculated the ratio of LF to HF. Total power, which is the highest peak in the frequency domain and within the frequency range of less than 0.4 Hz, was also extracted from PPG signals.

5.2.3 Statistical Features

Ten statistical characteristics of bio-signals were extracted using a sliding window. Each window had 20 seconds of measurement. The statistical characteristics include average, standard deviation, maximum, minimum, range, variance, root mean square, squared crest factor, skewness, and kurtosis. The squared crest factor is a peak-to-average power ratio (PAPR) of the signal [BR15b]. The skewness measures the symmetry of probability distribution. The skewness of the perfectly symmetrical normal distribution is zero. A positively skewed result has a distribution with an elongated right tail, while a negatively skewed result has a left tail [RS10]. The kurtosis means peakedness and flatness of tail of probability distribution [RMK12]. A positive kurtosis represents lighter in the tail, while a negative kurtosis means thicker in the tail than the normal distribution [RS10]. We generated 1117 features for the PPG dataset, and 747 features for the gait dataset were generated through feature extraction.
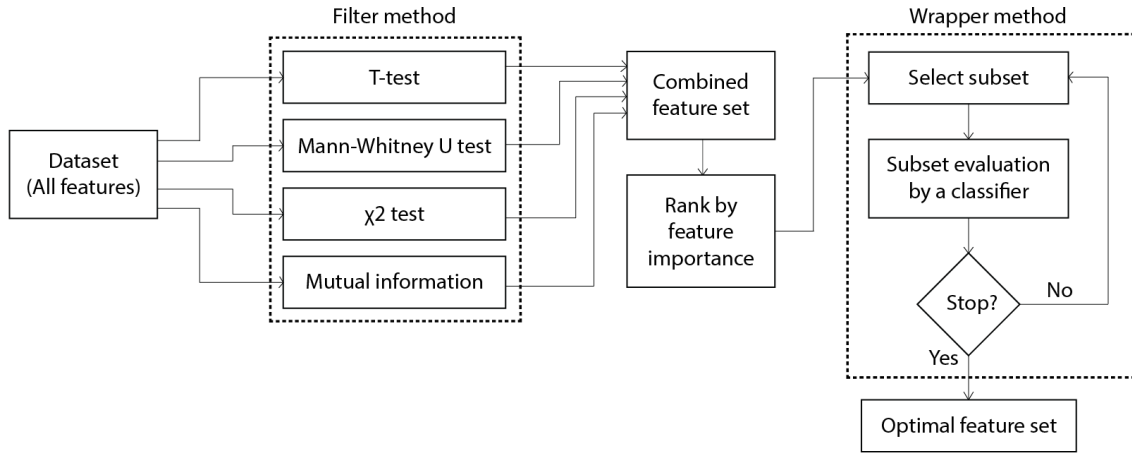
Figure 5.8: Feature selection algorithm for MCI classification using sensor-derived features.

5.3 Feature Selection

We designed a feature selection algorithm for the wearable sensor signal-derived features. Selecting an optimal subset of relevant features helps to avoid overfitting by high dimensionality and improves the learning performance [SIL07]. There are three methods for supervised feature selection: filter, wrapper, and embedded method. The filter method prunes low-scoring features, while the wrapper method searches for an optimal feature subset by evaluating each subset by the pre-determined classifier's predictive accuracy [WTL17]. The filter method only looks at the intrinsic properties of data, so it is easy to scale the very high dimensionality [SIL07]. In contrast, the wrapper method includes interaction with the selected classifier but requires a high computational cost to search in the space of possible feature subsets [SIL07]. The embedded method is a hybrid of both filter and wrapper method, which filters the features by the statistical criteria first, and then selects candidate subsets with a given cardinality [WTL17]. The embedded method is less computationally intensive than the wrapper method. A single feature selection method did not provide a remarkable classification result with our dataset, including features from signal processing.

We propose a feature selection algorithm to overcome the existing methods. The algo-

70

Table 5.2: Cross-validation classification accuracy of each feature selection in the PPG dataset

Model	All	CVLT-II	Filter	Wrapper
LR	0.59 (0.02)	0.78 (0.11)	**0.86 (0.05)**	0.82 (0.10)
KNN	0.47 (0.09)	0.80 (0.09)	0.69 (0.06)	**0.82 (0.07)**
RF	0.51 (0.09)	0.80 (0.06)	0.70 (0.14)	**0.90 (0.01)**
ET	0.63 (0.08)	0.78 (0.04)	0.70 (0.16)	**0.82 (0.08)**
NB	0.43 (0.14)	0.82 (0.07)	0.61 (0.10)	0.82 (0.08)
MLP	0.67 (0.04)	0.82 (0.07	0.84 (0.05)	**0.86 (0.05)**

rithm combines a filter method with ranking and a wrapper method with a forward approach. We selected top 30 features based on the score of four statistical hypothesis testing: T-test, Mann-Whitney U test, χ^2 test, and mutual information. We combined all the selected features without duplicates and reduced the dimensionality to 83 features. We ranked the filtered features by the feature importance based on Single Variable Classifier (SVC). The SVC ranking uses the predictive performance of a classifier built using only one feature [FSF14]. The PPG dataset used the Gini importance of the Extra-Trees (ET) for feature ranking. The Gini importance is measured by the total reduction of the Gini impurity brought by the selected feature [PVG11]. The gait dataset used the logistic regression coefficient for feature ranking.

With a forward approach, the wrapper method finalized the optimal feature set. The forward approach generated feature subsets by adding one feature sequentially. We used the ET as the classifier of the wrapper method. Our algorithm iterates over the ranked list only once to generate possible subsets. The algorithm selects the best feature set, which has the highest CV score.

Table 5.3: Cross-validation classification accuracy of each feature selection in the gait dataset

Model	All	CVLT-II	Filter	Wrapper
LR	0.54 (0.18)	0.76 (0.10)	0.78 (0.13)	**0.88 (0.12)**
KNN	0.47 (0.11)	0.81 (0.06)	0.74 (0.14)	0.77 (0.14)
RF	0.62 (0.19)	0.76 (0.06)	0.66 (0.17)	0.69 (0.17)
ET	0.48 (0.14)	0.83 (0.06)	0.76 (0.16)	0.78 (0.12)
NB	0.57 (0.09)	0.72 (0.14)	0.72 (0.16)	0.79 (0.08)
MLP	0.54 (0.13)	0.72 (0.14)	0.74 (0.09)	**0.86 (0.09)**

5.4 Experiment Results

The feature selection algorithm was evaluated with the six classification models: Logistic regression (LR), Random Forest (RF), ET, K-Nearest Neighbors (KNN), Naïve Bayes (NB), and Multilayer Perceptron (MLP). We evaluated each subset by the 5-fold Cross-Validation (CV) until including all features of the ranked list (Table 5.2 and Table 5.3). The Random Forest model fits several decision-tree models on various sub-samples of the dataset, while the Extra Trees model consists of randomized decision trees. The classification accuracy using all features is as low as randomly picking one between two targets. This result explains that some of the extracted features are noisy and redundant. We compared the classification accuracy of each step of feature selection with the classification accuracy only using the CVLT-II score, which has a high correlation (p-value; 5.7e-7) with the MCI diagnosed group. The classification accuracy is improved using the feature subset after the filter method but still not higher than using the CVLT-II score alone.

The KNN, RF, ET, and MLP classification models performed better with the optimal feature set than using the CVLT-II score alone with the PPG signal dataset. Interestingly, the LR classification model generated the best accuracy with the feature set after the fil-

ter method. The RF classifier's classification accuracy was remarkably increased with the optimal feature set after the wrapper method. With the gait dataset, the LR and MLP models with the optimal feature subset after the wrapper method provided better classification accuracy than using the CVLT-II score alone.

5.5 Discussion

The classification accuracy results explain that the feature extraction from bio-signals creates redundant features, and an optimal feature selection is crucial for successful classification. The proposed feature selection algorithm provides fast and straightforward execution for redundantly extracted features from PPG signals. The filter method by statistical hypothesis testing eliminates irrelevant features and reduces computational cost due to high dimensionality. The time complexity of the wrapper method is also reduced to $O(n)$, where n is the number of the ranked features.

The feature ranking before iterating the wrapper method was key to finding optimal feature subset effectively, compared to the genetic algorithm or the SFFS. The feature ranking is generally robust against overfitting and computationally efficient because it has less variance [GE03]. However, Fakhraei et al. [FSF14] demonstrated that SVC feature ranking alone for the bio-signal classification might not have an excellent predictive power because it is sensitive to the selection of classifiers. Some classifiers may experience a high loss of performance when used for both ranking and classification [FSF14]. Our PPG features used the Gini importance of ET for ranking, but the ET did not deliver remarkably higher performance. The ET may not be suitable to use for both ranking and classification.

The optimal feature set may represent essential predictors for the MCI classification. For example, maximum PPG values during the cognitive task and MeanPP of initial PPG were the top signal-derived features in the ranked list besides neuropsychological measures. These markers imply the amplitude of PPG signals with mental stress, and the intervals of PPG

peaks are significant markers to identify MCI aging. Also, kurtosis and range of PPG with mental stress were essential features for the MCI classification.

5.6 Conclusion

In this chapter, we proposed a novel application area of machine learning in the diagnosis of MCI. We were able to collect accelerometer, gyroscope, and PPG signals using a smartwatch and a wireless pulse oximeter with a connected smartphone. We explored indicators from bio-signals to recognize MCI. We applied several signal processing techniques to extract features from the sensor signals. We also demonstrated a new method of using the filter and wrapper methods to find the optimal feature subset. We evaluated selected features by several classification algorithms. Our experiment and the classification accuracy verify that the identification of MCI can be enhanced with sensor-derived features in addition to the administered neuropsychological measures. This application has the potential to be a reliable additional source of information for the detection of MCI in clinical settings and a quick initial assessment of cognitive change in high-risk populations in naturalistic settings using easy-access mobile, wearable devices. Furthermore, our feature selection algorithm has the potential to be a self-calibrating protocol in machine learning applications using bio-signals. Our proposed approach may produce social and economic benefits, including diagnosing with detailed analysis, providing optimized treatments, decreasing healthcare costs, and reducing the burden on families, caregivers, and doctors.

CHAPTER 6

Mental Health Monitoring with Passive Sensing

6.1 Objectives

Mental illness affects millions of people across the U.S. According to resources on the National Institute of Mental Health, in 2020, 52.9 million adults in the U.S. experienced mental illness, but only 24.3 million (46.2%) Americans have received mental health services [nim]. In addition, 14.2 million adults (or 5.6% of the U.S. population) had Serious Mental Illness (SMI) in 2020, resulting in severe functional impairment [nim].

Within the spectrum of mental health disorders, anxiety disorders are the most common class of psychiatric problems affecting both children and adults [BHG18, Car06, MHB10], with up to one in three people in the U.S. meeting full diagnostic criteria by early adulthood [TEW17, HHP08]. This fact manifests in the form of roughly 7 to 9% of the population in the U.S. suffering from a specific phobia, 7% from social anxiety disorder, and 2 to 3% each from panic disorder, agoraphobia, generalized anxiety disorder, and separation anxiety disorder [Ass19]. Individuals with anxiety disorders contend with substantial distress and impairment. They are at heightened risk for a host of negative long-term outcomes, including depression, substance abuse, educational underachievement, and poor physical health [NMW14, BMC98, WF01].

One of the major challenges in mental health treatment is the delay between the onset or worsening of symptoms and medical interventions. Typical psychiatric assessments, like clinical interviews and self-reports, require patients to report their past thoughts, feelings,

and behaviors in a clinical setting. The retrospective summaries can cause problems because the environment may cause them to misreport their information to their doctor. They might recall things inaccurately because of the delay between their symptoms and the assessment. Furthermore, the symptoms of mental illness often make it difficult to adhere to treatment plans, which can lead to a rapid decline in mental health, with potentially serious consequences such as eviction, job loss, incarceration, hospitalization, or even suicide. Changes in mental health can occur so quickly that it is challenging for psychiatrists to adjust their treatment effectively. Time-sensitive intervention is crucial to prevent it from being chronic with minimum cost. The optimal prevention or care for mental illness is early identification and diagnosis. This highlights the need for new strategies for psychiatrists to monitor patients' mental health remotely.

A recent alternative approach is that pervasive mental health monitoring is feasible through the embedded sensors on a smartphone, such as motion sensors, ambient light, microphone, camera, GPS, proximity, and touch screen. Furthermore, the touch screen display provides convenient user interfaces and interactions. The ubiquity of smartphones and digital devices amongst the general population presents a previously unavailable opportunity to explore an alternative approach to mitigating the risk of mental disorders. Moreover, recent smartphones have been evolving to embed advanced sensors, communications, and processing capabilities. The advantage of the smartphone-based platform, unlike traditional psychiatric assessments, is the detection of mental changes with a more reliable indicator of an individual's risk at any given time by operating it passively in the background of an individual's day-to-day life.

Research studies have been conducted to develop the capacity of passive sensing for mental illnesses. Previous passive data collection research in naturalistic settings has employed devices such as smartwatches or other wearable sensors both in conjunction with smartphones and independently of them, to monitor physical activities potentially linked to mental health [KW16]. In addition, utilizing wearable devices increases the accuracy [RD16]

due to their relative positioning on the body. For example, placement on the arm is a better indicator of motion. At the same time, smartphone-derived data presents several challenges. First, it is limited in their accuracy by the significant differences in behavioral patterns across users, such as age differences in usage profiles or age differences in the way of carrying the device. Second, smartphone-derived data brings unnecessary noise by tracking specific metrics indirectly. For instance, while embedded sensors are comparable to smartwatches in their ability to monitor activities, phones are often not worn directly when the user is active, complicating accurate classification.

Despite these challenges, a handful of studies have tracked self-reported depressive feelings against a range of passive sensing obtained through smartphones and have shown statistically significant relationships [WKF16, SZK15, WAA16, XLL13]. The metrics monitored vary from study to study, such as audio and light tracking, GPS, and call logs. However, in general, there has been a focus on physical activity, mobility, and sociability of users. Our work attempts to extend previous efforts in passive sensing of mental health. This chapter presents a novel system for the near-real-time risk assessment of mental health. We offer a systems implementation and an overview of an analytics framework, along with the specific results of an initial pilot study.

6.2 eWellness System Specification

We present a system for the remote monitoring of individuals' mental health symptoms, their fluctuation, and their attendant disruption to personal functioning, called eWellness. The eWellness framework is designed to capture a broad spectrum of remote monitoring, survey data acquisition, secure data transmission and management, data analytics, and visualization.

The primary component of eWellness is a mobile application that facilitates behavioral data collection and transmission harvested from an array of built-in sensors and usage logs

from a user's smartphone device. The data is collected passively, pre-processed, and transmitted to the cloud-based database. Concurrently the eWellness application includes an active querying component where the users can be prompted with Ecological Momentary Assessments (EMA) regarding their mental health status. EMA allows repeated sampling of thoughts, feelings, and behavior in near-in-time to the experience in naturalistic settings [GRN18]. This architecture is complemented by a back-end analytic engine, capable of mapping observed metrics and exogenous data sources to a user's mental health status, based on adaptive statistical models and advanced machine learning algorithms.

The eWellness mobile application captures the following metrics utilizing Aware [FK21], an open-source context instrumentation framework:

- **Application use**: is measured by frequency and duration of use of specific phone apps.

- **Social communication**: is monitored by incoming and outgoing phone calls and text messages, including the number of texts and phone calls and unique individuals contacted. This metric does not assess the content of communications or the recipient of the communication beyond establishing a unique contact.

- **Location**: is periodically sampled using GPS, network, and Wi-Fi detection. Prompts for a new location after moving 5 meters, up to once a minute. This metric leverages the Google Fused Location API. The application does not track specific locations; instead, it keeps a total distance traveled.

- **Ambient sound**: detects speech and communication above 50 decibels using the phone's microphone. It monitors every 5 minutes for 5 seconds. This metric does not assess the content of communications and merely records the decibel level in a numeric value.

- **Activity and movements**: leverage the device's accelerometer, gyroscope, and GPS
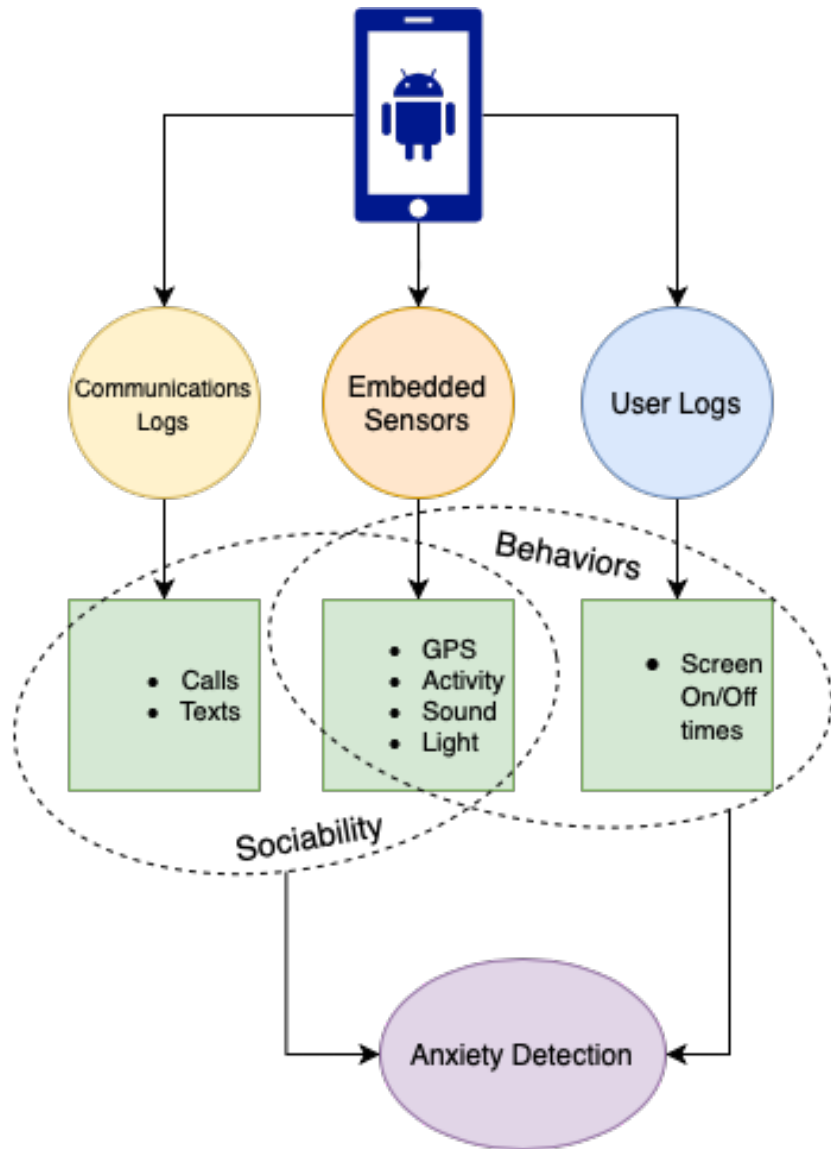
Figure 6.1: eWellness data collection hierarchy
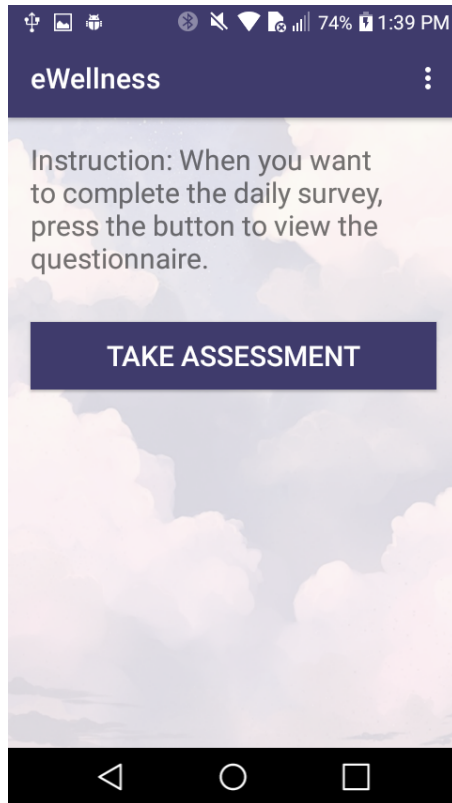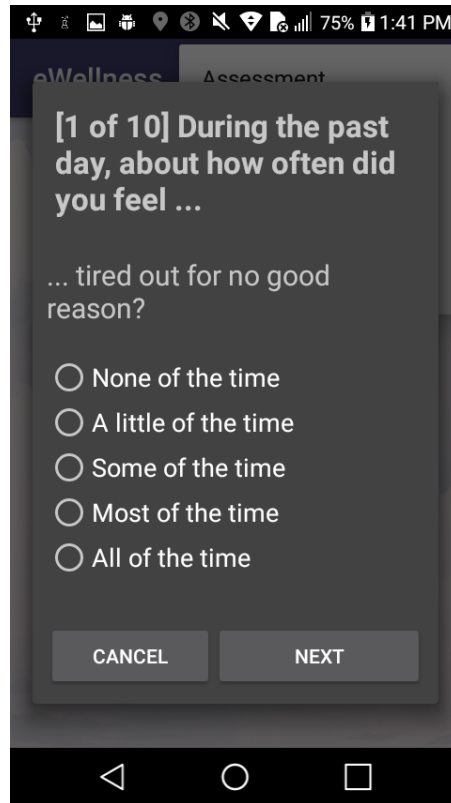
(a) Landing page.   (b) Daily EMA questionnaire.

Figure 6.2: eWellness app

tracking. Activity is sampled every 60 seconds. This metric leverages Google's Activity Recognition API to determine the activity type.

- **Light**: detects light level associated with possibly being in an outdoor or indoor location. This sensor is sampled every 6 seconds.

- **Phone use**: is user-log monitoring the device's screen on time.

Kessler Psychological Distress Scale (K10) [AS01] is a validated measure of psychological distress during the past 30 days, which is used for clinical and epidemiological purposes. It has notable success in measuring feelings of anxiety along with depression. The K10 has ten items, which are scored from five to one (all of the time, most of the time, some of

Table 6.1: Categorization of K10 score [aus].

K10 Score	Level	Samples (N=146)
10-15	Low distress	91
16-21	Moderate distress	29
22-29	High distress	21
30-50	Very high distress	5

the time, a little of the time, and none of the time). For the pilot study, the K10 was modified to assess criteria over the previous 24 hours. The minimum possible score of K10 is 10, and the maximum possible score is 50. K10 results are categorized into four levels of psychological distress: low distress, moderate distress, high distress, and very high distress. Table 6.1 details the stress threshold scores. These results were leveraged as a label for the classification of supervised learning.

6.3 Data Analytics

An IRB-approved pilot study was conducted on a dozen individuals who were recruited from the university community. Study participants did not have a reported history of mental illness. They were asked to download and install the eWellness Android application and then run it on their phone for a month. Participants were asked to answer EMA daily through the eWellness app. Only 10 participants answered at least seven days of EMAs and provided successful passive sensing data throughout the month. Our analysis focused on a fully supervised learning approach, and only labeled samples were included. We used 146 daily samples to identify daily anxiety and depression levels for this pilot study. The Z-Score normalization was applied to the features to reach normalized values from different participants.

We derived daily aggregated features from these metrics to infer both a user's sociability

and behavioral patterns from these raw values. These were then used to learn a model for the prediction of anxiety symptom severity. Statistical characteristics are obtained, such as minimum, maximum, mean, standard deviation. The 25th, 50th, and 75th percentiles of the numeric values of noise exposure and the ambient luminescence are also calculated. The number of activity transitions and duration of each physical activity per day also became a significant metric of identifying mentally distressed days. We selected 25 features with a relatively higher correlation with the raw K10 score. Table 6.2 provides a detailed list of feature labels and associated descriptions.

For the 4-class classification, we used 5-fold Cross-Validation (CV) with four classifiers: K-Nearest Neighbors (KNN), Extra-Trees (ET), Support Vector Machine (SVM), and Multi-layer Perceptron (MLP). The class weight was automatically applied to the models inversely proportional to the class frequencies to train the imbalanced dataset. The highest classification accuracy achieved for the four different stress levels was 76% with the extra-trees model. For another approach to complement the imbalanced dataset issue, we also applied the under-sampling technique. Samples from the low distress class were removed randomly to make uniformly distributed class labels. Samples from the very high distress class were also ignored due to the small number of samples. A confusion-matrix (Figure 6.3) demonstrates that the average score of classifying three classes is 0.65.

6.4 Discussion

6.4.1 Relevant Features

There are some notable and counter-intuitive findings regarding what data elements proved to be most highly correlated to mental health. It is not surprising to note the presence of features closely related to physical activities, like duration of time spent biking or walking, as such activities have been linked to mental health [Ste88].

What is somewhat less intuitive is the presence of multiple audio and light sensing fea-

Table 6.2: Most highly correlated features to K10 scores

Feature Name	Description
total-messages	Total # of text messages-received
is-silent-count	Number of instances no noise was detected
freq-std	Standard deviation for noise frequency
freq-25%	Noise frequency 25th percentile value
deci-std	Standard deviation for noise decibel
deci-50%	Noise decibel 50th percentile value
deci-75%	Noise decibel 75th percentile value
rms-max	Root mean squared measure of audio over time
act-transition	Activity tracking count when in transition
still-cnt	Total count of time user was still
tilting-cnt	Total count of instances the user was tilting
on-foot-cnt	Total count of the instances the user was still
on-bicycle-cnt	Total count of time user was riding a bike
on-foot-dur	Duration of time on foot
on-bicycle-dur	The duration the user spent on a bike
elapsed-device-on	Count of time the phone was active
elapsed-device-off	Count of time the phone was inactive
light-std	Standard deviation for luminescence value
light-25%	Luminescence 25th percentile value
light-50%	Luminescence 50th percentile value
loc-speed-mean	Average speed traveled in a day
loc-alt-mean	Mean Altitude Location
loc-alt-std	Standard deviation od the altitude
loc-alt-75%	Altitude 75th percentile value
loc-alt-max	Altitude max value
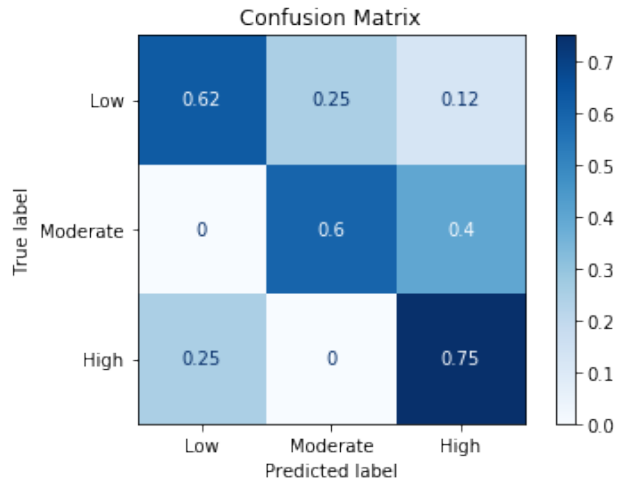
Figure 6.3: Confusion matrix of 3-class (Low, Moderate, and High distress) Classification.

tures. Audio sensing was included in the protocol under the hypothesis that a moderate level of sound could indicate pro-social activities like being outdoors or in group settings. Conversely, overly loud or quiet noise profiles could show stressful environments or isolated conditions that could harm mental health. But while interesting in theory, there are many confounding causes of noise that we would fail to distinguish by limiting ourselves to solely capturing the frequency and decibel levels of the sound. Intuitively, someone watching TV at home alone could register the same noise profile as someone out to dinner with friends.

Similarly, it was hypothesized that light sensing could be indicative of an individual being outside, which has been shown to correlate to mental health positively [TDC15]. However, here too, many confounding factors impacted light readings, foremost that the user would have to have their phone out and exposed when outside for the light sensor to register it. We suggest additional work is needed to understand whether these features are more universally indicative of mental health and explore why that is potentially the case.

6.4.2 Privacy Protection

A common concern about passive monitoring is the invasiveness and pervasiveness of the data collection. It may be inhibiting some individuals from participating in the program. Data collection was carefully scoped to avoid collecting Personally Identifiable Information (PII) that could link to a particular user. For example, when attempting to measure sociability, the application logs the total number of phone calls made, total time on the phone, and the number of unique contacts called; the identities of specific callers were not tracked. As a result, the application is unable to differentiate between calls to friends and calls to a customer service hotline. PII has the consequence of introducing a degree of obscurity into an observed finding. Limiting the PII data collection was necessary to respect privacy and ensure the app's acceptability. Likewise, although location data, such as placing at home or a recreational site, can be a valuable indicator of mental health, the PII associated with storing such information was deemed too intrusive. So location analysis was limited solely to a count of total distance traveled.

6.4.3 Usability

Attempting to gauge the viability of the concept, participants in the pilot were asked to submit a voluntary anonymized post-study questionnaire regarding their perceptions about the application and its data collection practices. All participants responded. A significant majority described the application as somewhat (40%) or mostly (40%) useful. Likewise, all users endorsed feeling comfortable with the application, and only one user expressed reservations about the data being collected.

All participants obtained detailed accounting of the data that was collected as part of their onboarding process to the study. No individual declined to participate after learning the precise nature of what was being tracked. This sampling suggests that there is less concern about data collection through their mobile devices, particularly among the young

adults who are more accustomed to digitized lives. Limiting the collection of PII could be sufficient to assuage most privacy concerns.

The primary issue that the users had with the application was its battery consumption resulting from heavy over-sampling of the sensors. As a result, future iterations of the application will seek to optimize battery usage by minimizing the sampling frequency.

6.4.4 Limitations of Dataset

While 10 subjects completing one month of continuous data represents a critical validation of the technology and its potential utility, the dataset is too small to achieve statistically significant results. There were insufficient cases of user-reported mental distress, particularly moderate or severe cases, in order to classify them effectively. Additional studies are planned to enlarge our dataset and include a cohort of individuals with diagnosed mental health conditions.

6.5 Conclusion

Remote health monitoring of mental health, when done so leveraging passive and unobtrusive data collection, could be a useful alternative for conducting real-time mental health surveillance. This chapter presents eWellness, an experimental mobile application designed to track a full suite of sensors and log data off a user's device continuously and passively. An initial pilot study tracking ten people over a month showed a nearly 76% success rate at predicting daily anxiety levels based solely on the passively monitored features. Our current approach may prove useful at tracking longitudinal trends in an individual's mental health and providing a platform for just-in-time interventions to mental health crises. However, additional work is needed to refine both the technology and analytics.

CHAPTER 7

Conclusion

7.1 Summary

This dissertation presented various IoT-enabled health monitoring systems to prove the benefits of H-IoT applications. In addition, this dissertation proposed possible technical solutions to resolve existing medical and healthcare problems in vital sign assessment, physical activity tracking, and mental stress monitoring. These RHM systems are developed in conjunction with the Computer Science department at the University of California, Los Angeles (UCLA), UCLA Easton Center for Alzheimer's Disease Research, Digital Health Lab at Samsung Research America (SRA), Orthopaedic Institute of Children's Health of Orange County (CHOC), Physical Therapy department at Chapman University, and the Mitre Corporation. This dissertation made the following contributions:

- Development of several remote health monitoring systems to solve medical and health problems

- Deployment of the system for clinical trials

- Investigation of system validation

- Design of health data analytics including signal processing, feature extraction, prediction modeling.

7.2 Challenges

Many IoT challenges and open issues remain in improving the quality of services (QoS) and end-users' requirements. The QoS metrics to evaluate the IoT system can include functional stability, performance, security, privacy, compatibility/interoperability, and scalability [PRW21]. The introduced applications from previous chapters mainly focused on developing affordable, portable, easy-to-install, and easy-to-use sensing devices or platforms for end-users. However, IoT-enabled systems can face potential performance bottlenecks, such as transmission delays, memory leakage, battery drainage, and security threats as the number of users grow. Therefore, systems with low latency, low power operation, high security, interoperability, and scalability will lead to increased adoption and acceptance by end-users of IoT-based RHM systems.

The IoT-based RHM systems require data sharing and transfer between multiple places for a virtual consultation [PRW21]. Transferring data between various sensors in the things layer to the processing node with low latency enables RHM applications to deliver the real-time intervention. For example, the alert generating system for chronic patients is crucial to process data from connected devices and provide a warning at the right moment. However, increased data size to improve detection accuracy may cause longer transmission delays with the current wireless network. Supporting mobility of body sensors is also a critical challenge in IoT-enabled RHM systems because network performance decreases as soon as the user moves to different locations [QNZ20]. The transmission delay can be reduced with high bandwidth and availability. Among short communication modalities for H-IoT, WiFi particularly uses the highest transmission power but affects the available bandwidth of other surrounding wireless devices [PRW21]. Wireless interference issue is another research topic to improve unexpected disconnections, poor signal strength, and transmission delays [PRW21]. We need further improvement in the performance of WBAN and WPAN networking.

Energy constraints and battery recharging are critical challenges to operate continuous

data acquisition and processing in the sensors or things layer. For example, current wearable devices or fitness trackers need to recharge after a period of usage, which causes disconnection for constant monitoring for at least a few minutes or hours. Even more, batteries on implantable devices cannot be replaced or recharged often [QNZ20]. In addition, device operations with low power can generate wireless interference and functional instability [PRW21]. Recently, some studies have introduced battery-less operation or deriving energy from the human body [QNZ20]. However, the implementation cost or any harmful side effects need more investigation [QNZ20]. Therefore, developing long-lasting battery sources is inevitable to increase operational stability and system reliability.

Ensuring the security and privacy of the user's sensitive health data is essential for IoT-based RHM systems. We all have the right to maintain an individual's privacy from public life. Electronic health records (EHR), personal health records (PHR), personal identifiable information (PII), medical lab results, vital signs, and biosignals are all important personal information that should be protected from identity theft and possible criminal attacks. For example, prescription information can be used to order prescription drugs for an enormous profit in the Dark Web marketplaces [Fue17]. In addition, PII, like social security numbers or medical insurance ID, can be used to create fake identities [Fue17]. Therefore, developers need to ensure employing all possible security mechanisms or privacy policies on every component of IoT systems, such as encryption, authorization, authentications, and anonymization [PRW21]. There are strict regulatory requirements for healthcare data protection, such as Health Insurance Portability and Accountability Act (HIPAA) and the EU General Data Protection Regulation (GDPR). However, more robust regulations about data accessibility are required, like secondary use of the collected data [PRW21].

A computer scientist, Peter Wegner defines the term interoperability as *"the ability of two or more software components to cooperate despite differences in language, interface, and execution platform"* [Weg96]. Achieving interoperability in language, interface, and platform will encourage a massive deployment of RHM applications. Monitoring functionality

and the user interface for various RHM applications are mostly similar, but implementing each application in different languages, interfaces, and platforms creates another burden on software development and maintenance. For example, in the previous chapters, proposed applications mostly used an Android device for the user interface for the connected devices because Android compatible devices are a more affordable option for clinical trials and developing costs. Moreover, heterogeneous IoT sensors, devices, applications, and services involve heterogeneous data formats [PRW21]. However, there are no standardized data formats to integrate the systems fully.

The volume of data from multiple sensors, devices, applications, and services is generated every second in the remote monitoring systems. According to the survey by Yousefpour et al. [YFN19], 2.5 exabytes of new digital data have been generated every day since 2012. The labeled data, or ground truth, is an essential source of supervised learning algorithms to generate massive training sets. Such training sets are a significant upfront cost of deep learning to reach predictive performance [RBE19]. However, obtaining high-quality data labels is enormously expensive. It is a time-consuming process and often requires domain expertise. In addition, as the number of connected devices increases, exposure to electromagnetic radiation by convolving multiple communication technologies must be considered as a possible hazard to the human body [QNZ20].

7.3 Future Research Direction and Trends

In recent years, many recommendations and future directions of technologies, such as edge/fog computing, AI/ML/DL, blockchain, and software-defined networks (SDN), have been proposed to complement current challenges in IoT-enabled RHM systems. The combination of multiple technologies can improve system performance significantly [QNZ20].

Taking the computing paradigm closer to the connected devices and away from the centralized cloud server can resolve many challenges in IoT. Fog computing is located between

the cloud and end nodes, while edge computing is located at the edge of the network close to end nodes, the things layer [YFN19]. Edge computing enables local computation and storage in the things layer to reduce data transmission time and power consumption [QNZ20]. Distributed architecture, as in the case of fog and edge computing systems, may offer a highly effective reduction in the processing delay and power consumption of devices in the things layer. Moreover, fog/edge computing can enhance security and optimize network traffic and bandwidth utilization [QNZ20].

Machine learning algorithms and big data analytics have been matured and applied to all the research fields. The IoT-based RHM applications presented in the previous chapters already explored various machine learning techniques. Still, various artificial intelligence (AI) techniques can be applied to deliver even better healthcare services. Massive data from in-clinic or in-home, such as electronic health records (EHR), lab results, and history of sensor data, are available to aid decision support systems for healthcare professionals so they can make a better diagnosis and personalized treatment [PRW21]. Efficient data preparation is necessary to reduce the burden of big data management and analytics as data size grows. Data quality assurance offers efficient data processing in RHM and an extensive understanding of human behavior and health.

Blockchain is one of the top trending technologies as a transparent data storage system because it supports distributed and completely decentralized peer-to-peer data transferring [QNZ20]. Each data block in blockchain or each change in the block generates a unique hash, which is used to maintain the chain of the block. A proof-of-work or a complex mathematical problem validates the distributed block in the chain [QNZ20]. Blockchain has been mostly applied in cryptocurrency but also can benefit current healthcare systems by offering decentralization, integrity, and anonymity [QNZ20]. Storing and securely controlling personal medical data is feasible, but further research is still required to utilize blockchain in healthcare.

Traditional network management depended on the pre-programmed, predetermined oper-

91

ations on the network devices, such as routers, switches, and intermediary devices [QNZ20]. However, this kind of network architecture cannot support flexibility, reconfiguration, and interoperability with the tremendous increase of network size and diversity [QNZ20]. Software-defined network (SDN) separates network control from hardware devices by making network devices forwarding only and configuring the network in the centralized controller [QNZ20]. Therefore, SDN can complement many network challenges in IoT systems, such as energy management and network security.

Overall, IoT-enabled health monitoring matures with the development of sensing, information, and communication technologies. The deployed wearables, body implements, and environmental sensors continuously collect the end user's health and wellness status. The medical institute's cloud services or data centers process the collected data and provide optimal healthcare services. The wireless network protocols link numerous users and medical professionals with the connected devices. We still need further research and analysis to fulfill the QoS requirements in RHM systems. As IoT technology develops, the large-scale adoption of IoT-enabled RHM applications is inevitable. There is great potential to shift from healthcare services within the clinical setting to a satisfactory user-centered setting. Eventually, IoT-enabled RHM systems will reduce current healthcare burdens and encourage positive health outcomes for all populations.

REFERENCES

[ada19]   lady ada. "Adafruit Feather M0 Bluefruit LE.", [Accessed: 20-Jan-2019].

[Alb21]   Osamah Shihab Ahmed Albahrey. "Smart home-based IoT for real-time and secure remote health monitoring of triage and priority system using body sensors: multi-driven systematic review." 2021.

[AM08]   Charles Abraham and Susan Michie. "A taxonomy of behavior change techniques used in interventions." *Health psychology*, **27**(3):379, 2008.

[Ani19]   AnilM3. "Arduino IMU: Pitch & Roll from an Accelerometer.", Jan 2019.

[AS01]   Gavin Andrews and Tim Slade. "Interpreting scores on the Kessler psychological distress scale (K10)." *Australian and New Zealand journal of public health*, **25**(6):494–497, 2001.

[Ass19]   American Psychological Association. "What Are Anxiety Disorders?" `https://www.psychiatry.org/patients-families/anxiety-disorders/what-are-anxiety-disordersg`, 2019.

[aus]   "Chapter - K10 Scoring.".

[AYV18]   Arif Reza Anwary, Hongnian Yu, and Michael Vassallo. "Optimal foot location for placing wearable IMU sensors and automatic feature extraction for gait analysis." *IEEE Sensors Journal*, **18**(6):2555–2567, 2018.

[b22]   "Accelerometers.".

[BA99]   J Martin Bland and Douglas G Altman. "Measuring agreement in method comparison studies." *Statistical methods in medical research*, **8**(2):135–160, 1999.

[BDG13]   Guha Balakrishnan, Fredo Durand, and John Guttag. "Detecting pulse from head motions in video." In *Proceedings of the IEEE Conference on Computer Vision and Pattern Recognition*, pp. 3430–3437, 2013.

[BGM08]   Valentina Bianchi, Ferdinando Grossi, Guido Matrella, Ilaria De Munari, and Paolo Ciampolini. "Fall detection and gait analysis in a smart home environment." *Gerontechnology*, **7**(2):73, 2008.

[BHG18]   Rebecca H Bitsko, Joseph R Holbrook, Reem M Ghandour, Stephen J Blumberg, Susanna N Visser, Ruth Perou, and John T Walkup. "Epidemiology and impact of health care provider–diagnosed anxiety and depression among US children." *Journal of developmental and behavioral pediatrics: JDBP*, **39**(5):395, 2018.

[BMC98]   Anna M Bardone, Terrie E Moffitt, Avshalom Caspi, Nigel Dickson, Warren R Stanton, and Phil A Silva. "Adult physical health outcomes of adolescent girls with conduct disorder, depression, and anxiety." *Journal of the American Academy of Child & Adolescent Psychiatry*, **37**(6):594–601, 1998.

[BR15a]   Tony Beltramelli and Sebastian Risi. "Deep-spying: Spying using smartwatch and deep learning." *arXiv preprint arXiv:1512.05616*, 2015.

[BR15b]   Tony Beltramelli and Sebastian Risi. "Deep-spying: Spying using smartwatch and deep learning." *arXiv preprint arXiv:1512.05616*, 2015.

[BSW15]   Dror Ben-Zeev, Emily A Scherer, Rui Wang, Haiyi Xie, and Andrew T Campbell. "Next-generation psychiatric assessment: Using smartphone sensors to monitor behavior and mental health." *Psychiatric rehabilitation journal*, **38**(3):218, 2015.

[BV02]   Jennifer S Brach and Jessie M VanSwearingen. "Physical impairment and disability: relationship to performance of activities of daily living in community-dwelling older men." *Physical therapy*, **82**(8):752–761, 2002.

[CAE19]   Yekta Said Can, Bert Arnrich, and Cem Ersoy. "Stress detection in daily life scenarios using smart phones and wearable sensors: A survey." *Journal of biomedical informatics*, p. 103139, 2019.

[Car06]   Sam Cartwright-Hatton. "Anxiety of childhood and adolescence: Challenges and opportunities.", 2006.

[CKC21]   Daniel Carter, Juraj Kolencik, and Juraj Cug. "Smart Internet of Things-enabled Mobile-based Health Monitoring Systems and Medical Big Data in COVID-19 Telemedicine." *American Journal of Medical Research*, **8**(1):20–29, 2021.

[CLT16]   Nicola Carbonaro, Federico Lorussi, and Alessandro Tognetti. "Assessment of a smart sensing shoe for gait phase detection in level walking." *Electronics*, **5**(4):78, 2016.

[Coo19]   CoolThings. "Storage soles shoe insoles with hidden storage.", Jan 2019.

[CS82]   Charles S Carver and Michael F Scheier. "Control theory: A useful conceptual framework for personality–social, clinical, and health psychology." *Psychological bulletin*, **92**(1):111, 1982.

[CSY10]   Elaine Clark, Jane K Sweeney, Allison Yocum, and Sarah W McCoy. "Effects of motor control intervention for children with idiopathic toe walking: a 5-case series." *Pediatric Physical Therapy*, **22**(4):417–426, 2010.

[DBH18]   Karen Davies, Alec Black, Michael Hunt, and Liisa Holsti. "Long-term gait outcomes following conservative management of idiopathic toe walking." *Gait & posture*, **62**:214–219, 2018.

[DE13]   Ryan P Duncan and Gammon M Earhart. "Four square step test performance in people with Parkinson disease." *Journal of Neurologic Physical Therapy*, **37**(1):2–8, 2013.

[DJ13]   Gerard De Haan and Vincent Jeanne. "Robust pulse rate from chrominance-based rPPG." *IEEE Transactions on Biomedical Engineering*, **60**(10):2878–2886, 2013.

[DM17]   Hugo Dinis and Paulo M Mendes. "Recent advances on implantable wireless sensor networks." *Wireless sensor networks-insights and innovations*, 2017.

[DMH14]   Moran Dorfman, Anat Mirelman, Jeffrey M Hausdorff, and Nir Giladi. "Gait disorders in patients with cognitive impairment or dementia." In *Movement disorders in dementias*, pp. 17–44. Springer, 2014.

[DMW09]   Stefan Duschek, Magdalena Muckenthaler, Natalie Werner, and Gustavo A. Reyes Del Paso. "Relationships between features of autonomic cardiovascular control and cognitive performance." *Biological Psychology*, **81**(2):110–117, 2009.

[DPR19]   Fredrik Dahlqvist, Mark Patel, Alexander Rajko, and Jonathan Shulman. "Growing opportunities in the Internet of Things." *McKinsey & Company*, pp. 1–6, 2019.

[EGU11]   Raoul Engelbert, Jan Willem Gorter, Cuno Uiterwaal, Elise van de Putte, and Paul Helders. "Idiopathic toe-walking in children, adolescents and young adults: a matter of local or generalised stiffness?" *BMC Musculoskeletal Disorders*, **12**(1):61, 2011.

[Ele96]   Task Force Of The European Society Electrophysiology. "Heart Rate Variability." *Circulation*, **93**(5):1043–1065, 1996.

[EMD00]   Deborah M Eastwood, Malcolm B Menelaus, DR Dickens, Nigel S Broughton, and William G Cole. "Idiopathic toe-walking: does treatment alter the natural history?" *Journal of pediatric orthopedics. Part B*, **9**(1):47–49, 2000.

[FK21]   D Ferreira and V Kostakos. "Aware: Open-source context instrumentation framework for everyone." *URL: https://awareframework. com/.(Accessed: 2021-05-01)*, 2021.

[FSF14]   Shobeir Fakhraei, Hamid Soltanian-Zadeh, and Farshad Fotouhi. "Bias and stability of single variable classifiers for feature ranking and selection." *Expert Systems with Applications*, **41**(15):6945–6958, 2014.

[Fue17]   Mayra Rosario Fuentes. "Cybercrime and other threats faced by the healthcare industry." *Trend Micro*, 2017.

[GE03]   Isabelle Guyon and André Elisseeff. "An introduction to variable and feature selection." *Journal of machine learning research*, **3**(Mar):1157–1182, 2003.

[GFE19]   Migyeong Gwak, Shayan Fazeli, Ghazaal Ershadi, Majid Sarrafzadeh, Melina Ghodsi, Afshin Aminian, and John A Schlechter. "EXTRA: Exercise Tracking and Analysis Platform for Remote-monitoring of Knee Rehabilitation." In *2019 IEEE 16th International Conference on Wearable and Implantable Body Sensor Networks (BSN)*, pp. 1–4. IEEE, 2019.

[GH01]   Murray Goldstein and Dennis C Harper. "Management of cerebral palsy: equinus gait." *Developmental medicine and child neurology*, **43**(8):563–569, 2001.

[GRN18]   Enrique Garcia-Ceja, Michael Riegler, Tine Nordgreen, Petter Jakobsen, Ketil J Oedegaard, and Jim Tørresen. "Mental health monitoring with multimodal sensing and machine learning: A survey." *Pervasive and Mobile Computing*, **51**:1–26, 2018.

[GWS18a]   Migyeong Gwak, Ellen Woo, and Majid Sarrafzadeh. "The Role of Accelerometer and Gyroscope Sensors in Identification of Mild Cognitive Impairment." *IEEE Global Conference on Signal and Information Processing (GlobalSIP '18)*, 2018.

[GWS18b]   Migyeong Gwak, Ellen Woo, and Majid Sarrafzadeh. "The role of accelerometer and gyroscope sensors in identification of mild cognitive impairment." In *2018 IEEE Global Conference on Signal and Information Processing (GlobalSIP)*, pp. 434–438. IEEE, 2018.

[HBH16]   Siti Farah Hussin, Gauri Birasamy, and Zunainah Hamid. "Design of Butterworth Band-Pass Filter." *Politeknik & Kolej Komuniti Journal of Engineering and Technology*, **1**(1), 2016.

[HBL18]   Nadine Hochhausen, Carina Barbosa Pereira, Steffen Leonhardt, Rolf Rossaint, and Michael Czaplik. "Estimating respiratory rate in post-anesthesia care unit patients using infrared thermography: an observational study." *Sensors*, **18**(5):1618, 2018.

[HHP08]   Paul Hammerness, Theresa Harpold, Carter Petty, Chantal Menard, Claire Zar-Kessler, and Joseph Biederman. "Characterizing non-OCD anxiety disorders in psychiatrically referred children and adolescents." *Journal of affective disorders*, **105**(1-3):213–219, 2008.

[HJT03]   Anita Lill Hansen, Bjørn Helge Johnsen, and Julian F Thayer. "Vagal influence on working memory and attention." *International journal of psychophysiology*, **48**(3):263–274, 2003.

[HMB20]   Micah Hartman, Anne B Martin, Joseph Benson, Aaron Catlin, and National Health Expenditure Accounts Team. "National Health Care Spending In 2018: Growth Driven By Accelerations In Medicare And Private Insurance Spending: US health care spending increased 4.6 percent to reach \$3.6 trillion in 2018, a faster growth rate than that of 4.2 percent in 2017 but the same rate as in 2016." *Health Affairs*, **39**(1):8–17, 2020.

[HMR07]   Adélaïde van den Hecke, Christine Malghem, Anne Renders, Christine Detrembleur, Sara Palumbo, and Thierry M Lejeune. "Mechanical work, energetic cost, and gait efficiency in children with cerebral palsy." *Journal of Pediatric Orthopaedics*, **27**(6):643–647, 2007.

[HW04]   Georg Hirsch and B Wagner. "The natural history of idiopathic toe-walking: a long-term follow-up of fourteen conservatively treated children." *Acta paediatrica*, **93**(2):196–199, 2004.

[HZU17]   Nagaraj Hegde, Ting Zhang, Gitendra Uswatte, Edward Taub, Joydip Barman, Staci McKay, Andrea Taylor, David M Morris, Angi Griffin, and Edward S Sazonov. "The pediatric SmartShoe: wearable sensor system for ambulatory monitoring of physical activity and gait." *IEEE transactions on neural systems and rehabilitation engineering*, **26**(2):477–486, 2017.

[ILC19]   Luca Iozza, Jesús Lázaro, Luca Cerina, Davide Silvestri, Luca Mainardi, Pablo Laguna, and Eduardo Gil. "Monitoring breathing rate by fusing the physiological impact of respiration on video-photoplethysmogram with head movements." *Physiological measurement*, **40**(9):094002, 2019.

[Ind]   Adafruit Industries. "Conductive Rubber Cord Stretch Sensor extras!".

[INM14]   Ramin Irani, Kamal Nasrollahi, and Thomas B Moeslund. "Improved pulse detection from head motions using DCT." In *2014 international conference on computer vision theory and applications (VISAPP)*, volume 3, pp. 118–124. IEEE, 2014.

[IRA21]   Bashima Islam, Md Mahbubur Rahman, Tousif Ahmed, Mohsin Yusuf Ahmed, Md Mehedi Hasan, Viswam Nathan, Korosh Vatanparvar, Ebrahim Nemati, Jilong Kuang, and Jun Alex Gao. "BreathTrack: Detecting Regular Breathing Phases from Unannotated Acoustic Data Captured by a Smartphone." *Proceedings of the ACM on Interactive, Mobile, Wearable and Ubiquitous Technologies*, **5**(3):1–22, 2021.

[JW15]   Andrew H. Johnston and Gary M. Weiss. "Smartwatch-based biometric gait recognition." *2015 IEEE 7th International Conference on Biometrics Theory, Applications and Systems (BTAS)*, 2015.

[JWM15] Rik Janssen, Wenjin Wang, Andreia Moço, and Gerard De Haan. "Video-based respiration monitoring with automatic region of interest detection." *Physiological measurement*, **37**(1):100, 2015.

[KMO21] Agni Kumar, Vikramjit Mitra, Carolyn Oliver, Adeeti Ullal, Matt Biddulph, and Irida Mance. "Estimating Respiratory Rate From Breath Audio Obtained Through Wearable Microphones." *arXiv preprint arXiv:2107.14028*, 2021.

[KMS11] Sander Koelstra, Christian Muhl, Mohammad Soleymani, Jong-Seok Lee, Ashkan Yazdani, Touradj Ebrahimi, Thierry Pun, Anton Nijholt, and Ioannis Patras. "Deap: A database for emotion analysis; using physiological signals." *IEEE transactions on affective computing*, **3**(1):18–31, 2011.

[KPB14] A Reşit Kavsaoğlu, Kemal Polat, and M Recep Bozkurt. "A novel feature ranking algorithm for biometric recognition with PPG signals." *Computers in biology and medicine*, **49**:1–14, 2014.

[KW16] Maulik R Kamdar and Michelle J Wu. "PRISM: a data-driven platform for monitoring mental health." In *Biocomputing 2016: Proceedings of the Pacific Symposium*, pp. 333–344. World Scientific, 2016.

[LBS04] S Li, M Bishop, C Senesac, R Woo, and M Horodyski. "The effect of botulinum toxin type A combined with physical therapy on gait in children with idiopathic toe walking." *Pediatr Phys Ther*, **16**:59, 2004.

[LCT16] Kuan-Yi Lin, Duan-Yu Chen, and Wen-Jiin Tsai. "Image-based motion-tolerant remote respiratory rate evaluation." *IEEE Sensors Journal*, **16**(9):3263–3271, 2016.

[Lew95] James R Lewis. "IBM computer usability satisfaction questionnaires: psychometric evaluation and instructions for use." *International Journal of Human-Computer Interaction*, **7**(1):57–78, 1995.

[LKB98] Guoan Li, Kenji Kawamura, Peter Barrance, Edmund YS Chao, and Ken Kaufman. "Prediction of muscle recruitment and its effect on joint reaction forces during knee exercises." *Annals of biomedical engineering*, **26**(4):725–733, 1998.

[LM11] Mariano Llamedo and Juan Pablo Martínez. "Heartbeat Classification Using Feature Selection Driven by Database Generalization Criteria." *IEEE Transactions on Biomedical Engineering*, **58**(3):616–625, 2011.

[LT13] Markus Löffler and Andreas Tschiesner. "The Internet of Things and the future of manufacturing." *McKinsey & Company*, **4**, 2013.

[Lun01] Arnold M Lund. "Measuring usability with the use questionnaire12." *Usability interface*, **8**(2):3–6, 2001.

[LWM06]   Wood W Lovell, Robert B Winter, Raymond T Morrissy, and Stuart L Weinstein. *Lovell and Winter's pediatric orthopaedics*, volume 1. Lippincott Williams & Wilkins, 2006.

[LWZ16]   Feng Lin, Aosen Wang, Yan Zhuang, Machiko R Tomita, and Wenyao Xu. "Smart insole: A wearable sensor device for unobtrusive gait monitoring in daily life." *IEEE Transactions on Industrial Informatics*, **12**(6):2281–2291, 2016.

[MBN]   L.c. Molina, L. Belanche, and A. Nebot. "Feature selection algorithms: a survey and experimental evaluation." *2002 IEEE International Conference on Data Mining, 2002. Proceedings.*

[MCB15]   James Manyika, Michael Chui, Peter Bisson, Jonathan Woetzel, Richard Dobbs, Jacques Bughin, and Dan Aharon. "Unlocking the Potential of the Internet of Things." *McKinsey Global Institute*, **1**, 2015.

[MCK10]   Blake D McLean, Aaron J Coutts, Vince Kelly, Michael R McGuigan, and Stuart J Cormack. "Neuromuscular, endocrine, and perceptual fatigue responses during different length between-match microcycles in professional rugby league players." *International journal of sports physiology and performance*, **5**(3):367–383, 2010.

[MDF84]   Guy McKhann, David Drachman, Marshall Folstein, Robert Katzman, Donald Price, and Emanuel M Stadlan. "Clinical diagnosis of Alzheimer's disease: Report of the NINCDS-ADRDA Work Group* under the auspices of Department of Health and Human Services Task Force on Alzheimer's Disease." *Neurology*, **34**(7):939–939, 1984.

[MGM14]   Alvaro Muro-De-La-Herran, Begonya Garcia-Zapirain, and Amaia Mendez-Zorrilla. "Gait analysis methods: An overview of wearable and non-wearable systems, highlighting clinical applications." *Sensors*, **14**(2):3362–3394, 2014.

[MHB10]   Kathleen Ries Merikangas, Jian-ping He, Marcy Burstein, Sonja A Swanson, Shelli Avenevoli, Lihong Cui, Corina Benjet, Katholiki Georgiades, and Joel Swendsen. "Lifetime prevalence of mental disorders in US adolescents: results from the National Comorbidity Survey Replication–Adolescent Supplement (NCS-A)." *Journal of the American Academy of Child & Adolescent Psychiatry*, **49**(10):980–989, 2010.

[MIH13]   Aizan Masdar, BSKK Ibrahim, Dirman Hanafi, M Mahadi Abdul Jamil, and KAA Rahman. "Knee joint angle measurement system using gyroscope and flex-sensors for rehabilitation." In *The 6th 2013 Biomedical Engineering International Conference*, pp. 1–4. IEEE, 2013.

[MMD17]   Sumit Majumder, Tapas Mondal, and M Jamal Deen. "Wearable sensors for remote health monitoring." *Sensors*, **17**(1):130, 2017.

[MRD19]   Lakmini P Malasinghe, Naeem Ramzan, and Keshav Dahal. "Remote patient monitoring: a comprehensive study." *Journal of Ambient Intelligence and Humanized Computing*, **10**(1):57–76, 2019.

[MRS01]   VS Murthy, Sripad Ramamoorthy, Narayanan Srinivasan, Sriram Rajagopal, and M Mukunda Rao. "Analysis of photoplethysmographic signals of cardiovascular patients." In *Engineering in Medicine and Biology Society, 2001. Proceedings of the 23rd Annual International Conference of the IEEE*, volume 3, pp. 2204–2207. IEEE, 2001.

[MRS13]   Michelle M Mielke, Rosebud O Roberts, Rodolfo Savica, Ruth Cha, Dina I Drubach, Teresa Christianson, Vernon S Pankratz, Yonas E Geda, Mary M Machulda, Robert J Ivnik, et al. "Assessing the temporal relationship between cognition and gait: slow gait predicts cognitive decline in the Mayo Clinic Study of Aging." *Journals of Gerontology Series A: Biomedical Sciences and Medical Sciences*, **68**(8):929–937, 2013.

[MS20]   Arya Deo Mehta and Hemant Sharma. "Tracking Nostril Movement in Facial Video for Respiratory Rate Estimation." In *2020 11th International Conference on Computing, Communication and Networking Technologies (ICCCNT)*, pp. 1–6. IEEE, 2020.

[MSC19]   F Mazur, B Swoboda, HD Carl, C Lutter, M Engelhardt, MW Hoppe, T Hotfiel, and C Grim. "Plantar pressure changes in hindfoot relief devices of different designs." *Journal of experimental orthopaedics*, **6**(1):7, 2019.

[nim]   "Mental illness.".

[NMW14]   Jill M Newby, Louise Mewton, Alishia D Williams, and Gavin Andrews. "Effectiveness of transdiagnostic internet cognitive behavioural treatment for mixed anxiety and depression in primary care." *Journal of Affective Disorders*, **165**:45–52, 2014.

[Non]   Nonin. "Onyx II 9550 — Nonin." `https://www.nonin.com/products/9550/`. (Accessed on 01/22/2019).

[Pet04]   Ronald C Petersen. "Mild cognitive impairment as a diagnostic entity." *Journal of internal medicine*, **256**(3):183–194, 2004.

[PHV17]   Carina Barbosa Pereira, Konrad Heimann, Boudewijn Venema, Vladimir Blazek, Michael Czaplik, and Steffen Leonhardt. "Estimation of respiratory rate from thermal videos of preterm infants." In *2017 39th Annual International Conference of the IEEE Engineering in Medicine and Biology Society (EMBC)*, pp. 3818–3821. IEEE, 2017.

[PKK01]   Tapani Pöyhönen, Heikki Kyröläinen, Kari L Keskinen, Arto Hautala, Jukka Savolainen, and Esko Mälkiä. "Electromyographic and kinematic analysis of therapeutic knee exercises under water." *Clinical Biomechanics*, **16**(6):496–504, 2001.

[PPL12]   Angkoon Phinyomark, Pornchai Phukpattaranont, and Chusak Limsakul. "Feature reduction and selection for EMG signal classification." *Expert Systems with Applications*, **39**(8):7420–7431, 2012.

[PRW21]   Nada Y Philip, Joel JPC Rodrigues, Honggang Wang, Simon James Fong, and Jia Chen. "Internet of Things for in-home health monitoring systems: current advances, challenges and future directions." *IEEE Journal on Selected Areas in Communications*, **39**(2):300–310, 2021.

[PVG11]   F. Pedregosa, G. Varoquaux, A. Gramfort, V. Michel, B. Thirion, O. Grisel, M. Blondel, P. Prettenhofer, R. Weiss, V. Dubourg, J. Vanderplas, A. Passos, D. Cournapeau, M. Brucher, M. Perrot, and E. Duchesnay. "Scikit-learn: Machine Learning in Python." *Journal of Machine Learning Research*, **12**:2825–2830, 2011.

[QNZ20]   Yazdan Ahmad Qadri, Ali Nauman, Yousaf Bin Zikria, Athanasios V Vasilakos, and Sung Won Kim. "The future of healthcare internet of things: a survey of emerging technologies." *IEEE Communications Surveys & Tutorials*, **22**(2):1121–1167, 2020.

[QSG13]   Yongbin Qi, Cheong Boon Soh, Erry Gunawan, Kay-Soon Low, and Arash Maskooki. "Measurement of knee flexion/extension angle using wearable UWB radios." In *2013 35th Annual International Conference of the IEEE Engineering in Medicine and Biology Society (EMBC)*, pp. 7213–7216. IEEE, 2013.

[RBE19]   Alexander Ratner, Stephen H Bach, Henry Ehrenberg, Jason Fries, Sen Wu, and Christopher Ré. "Snorkel: Rapid training data creation with weak supervision." *The VLDB Journal*, pp. 1–22, 2019.

[RCW14]   Shaoqing Ren, Xudong Cao, Yichen Wei, and Jian Sun. "Face alignment at 3000 fps via regressing local binary features." In *Proceedings of the IEEE Conference on Computer Vision and Pattern Recognition*, pp. 1685–1692, 2014.

[RD16]   Blaine Reeder and Alexandria David. "Health at hand: A systematic review of smart watch uses for health and wellness." *Journal of biomedical informatics*, **63**:269–276, 2016.

[RMK12]   M. Raghu Ram, K. Venu Madhav, E. Hari Krishna, Nagarjuna Reddy Komalla, and K. Ashoka Reddy. "A Novel Approach for Motion Artifact Reduction in PPG Signals Based on AS-LMS Adaptive Filter." *IEEE Transactions on Instrumentation and Measurement*, **61**(5):1445–1457, 2012.

[RS10]   David Rindskopf and Mariya Shiyko. *Measures of Dispersion, Skewness and Kurtosis*, pp. 267–273. 12 2010.

[RSD16]   Joseph J Ruzbarsky, David Scher, and Emily Dodwell. "Toe walking: causes, epidemiology, assessment, and treatment." *Current opinion in pediatrics*, **28**(1):40–46, 2016.

[SA98]   Stephen J Stricker and Julie C Angulo. "Idiopathic toe walking: a comparison of treatment methods." *Journal of Pediatric Orthopaedics*, **18**(3):289–293, 1998.

[Sac09]   Silonie Sachdeva et al. "Fitzpatrick skin typing: Applications in dermatology." *Indian journal of dermatology, venereology and leprology*, **75**(1):93, 2009.

[SBK07]   M. Sabeti, R. Boostani, S.d. Katebi, and G.w. Price. "Selection of relevant features for EEG signal classification of schizophrenic patients." *Biomedical Signal Processing and Control*, **2**(2):122–134, 2007.

[SBO16]   Heli Sätilä, Anneli Beilmann, Päivi Olsén, Heli Helander, Mari Eskelinen, and Heini Huhtala. "Does botulinum toxin a treatment enhance the walking pattern in idiopathic toe-walking?" *Neuropediatrics*, **47**(03):162–168, 2016.

[SDH20]   Dhruv R Seshadri, Evan V Davies, Ethan R Harlow, Jeffrey J Hsu, Shanina C Knighton, Timothy A Walker, James E Voos, and Colin K Drummond. "Wearable sensors for COVID-19: a call to action to harness our digital infrastructure for remote patient monitoring and virtual assessments." *Frontiers in Digital Health*, **2**:8, 2020.

[SFH10]   Edward S Sazonov, George Fulk, James Hill, Yves Schutz, and Raymond Browning. "Monitoring of posture allocations and activities by a shoe-based wearable sensor." *IEEE Transactions on Biomedical Engineering*, **58**(4):983–990, 2010.

[SHZ20]   Pragya Sharma, Xiaonan Hui, Jianlin Zhou, Thomas B Conroy, and Edwin C Kan. "Wearable radio-frequency sensing of respiratory rate, respiratory volume, and heart rate." *NPJ digital medicine*, **3**(1):1–10, 2020.

[SIL07]   Yvan Saeys, Iñaki Inza, and Pedro Larrañaga. "A review of feature selection techniques in bioinformatics." *bioinformatics*, **23**(19):2507–2517, 2007.

[SJS08]   N. Selvaraj, A. Jaryal, J. Santhosh, K. K. Deepak, and S. Anand. "Assessment of heart rate variability derived from finger-tip photoplethysmography as compared to electrocardiography." *Journal of Medical Engineering & Technology*, **32**(6):479–484, 2008.

[SMA87]   Gary L Soderberg, Scott Duesterhaus Minor, Kevin Arnold, Thomas Henry, Joyce Kirchner Chatterson, Debra Ridenour Poppe, and Cheryl Wall. "Electromyographic analysis of knee exercises in healthy subjects and in patients with knee pathologies." *Physical therapy*, **67**(11):1691–1696, 1987.

[SMB19]   Fabian Schrumpf, Christoph Mönch, Gerold Bausch, and Mirco Fuchs. "Exploiting weak head movements for camera-based respiration detection." In *2019 41st Annual International Conference of the IEEE Engineering in Medicine and Biology Society (EMBC)*, pp. 6059–6062. IEEE, 2019.

[SN90]   K Donald Shelbourne and Paul Nitz. "Accelerated rehabilitation after anterior cruciate ligament reconstruction." *The American journal of sports medicine*, **18**(3):292–299, 1990.

[SSC97]   Lisa H Shulman, Debra A Sala, Mary Lynn Y Chu, Patricia R McCaul, and Bonnie J Sandler. "Developmental implications of idiopathic toe walking." *The Journal of pediatrics*, **130**(4):541–546, 1997.

[SSK99]   Debra A Sala, Lisa H Shulman, Rose F Kennedy, Alfred D Grant, and Mary Lynn Y Chu. "Idiopathic toe-walking: a review." *Developmental medicine and child neurology*, **41**(12):846–848, 1999.

[SSV11]   Amit Jasvant Shah, Shaoyong Su, Emir Veledar, James Douglas Bremner, Felicia C. Goldstein, Rachel Lampert, Jack Goldberg, and Viola Vaccarino. "Is Heart Rate Variability Related to Memory Performance in Middle-Aged Men?" *Psychosomatic Medicine*, **73**(6):475–482, 2011.

[Ste88]   Thomas Stephens. "Physical activity and mental health in the United States and Canada: evidence from four population surveys." *Preventive medicine*, **17**(1):35–47, 1988.

[SY13]   Li Shan and Minghui Yu. "Video-based heart rate measurement using head motion tracking and ICA." In *2013 6th International Congress on Image and Signal Processing (CISP)*, volume 1, pp. 160–164. IEEE, 2013.

[SZK15]   Sohrab Saeb, Mi Zhang, Christopher J Karr, Stephen M Schueller, Marya E Corden, Konrad P Kording, David C Mohr, et al. "Mobile phone sensor correlates of depressive symptom severity in daily-life behavior: an exploratory study." *Journal of medical Internet research*, **17**(7):e4273, 2015.

[TDC15]   Margarita Triguero-Mas, Payam Dadvand, Marta Cirach, David Martínez, Antonia Medina, Anna Mompart, Xavier Basagaña, Regina Gražulevičienė, and Mark J Nieuwenhuijsen. "Natural outdoor environments and mental and physical health: relationships and mechanisms." *Environment international*, **77**:35–41, 2015.

[TEA16]   Daniel Myklatun Tveit, Kjersti Engan, Ivar Austvoll, and Øyvind Meinich-Bache. "Motion based detection of respiration rate in infants using video." In *2016 IEEE International Conference on Image Processing (ICIP)*, pp. 1225–1229. IEEE, 2016.

[TEW17]   Maurice Topper, Paul MG Emmelkamp, Ed Watkins, and Thomas Ehring. "Prevention of anxiety disorders and depression by targeting excessive worry and rumination in adolescents and young adults: a randomized controlled trial." *Behaviour research and therapy*, **90**:123–136, 2017.

[TK91]   Carlo Tomasi and Takeo Kanade. "Detection and tracking of point." *Int J Comput Vis*, **9**:137–154, 1991.

[TVS09]   Joachim Taelman, S. Vandeput, A. Spaepen, and S. Van Huffel. "Influence of Mental Stress on Heart Rate and Heart Rate Variability." *IFMBE Proceedings 4th European Conference of the International Federation for Medical and Biological Engineering*, pp. 1366–1369, 2009.

[UHG17]   Jacek K Urbanek, Jaroslaw Harezlak, Nancy W Glynn, Tamara Harris, Ciprian Crainiceanu, and Vadim Zipunnikov. "Stride variability measures derived from wrist-and hip-worn accelerometers." *Gait & posture*, **52**:217–223, 2017.

[VJ01]   Paul Viola and Michael Jones. "Rapid object detection using a boosted cascade of simple features." In *Proceedings of the 2001 IEEE computer society conference on computer vision and pattern recognition. CVPR 2001*, volume 1, pp. I–I. Ieee, 2001.

[VWL07]   Joe Verghese, Cuiling Wang, Richard B Lipton, Roee Holtzer, and Xiaonan Xue. "Quantitative gait dysfunction and risk of cognitive decline and dementia." *Journal of Neurology, Neurosurgery & Psychiatry*, **78**(9):929–935, 2007.

[WAA16]   Rui Wang, Min SH Aung, Saeed Abdullah, Rachel Brian, Andrew T Campbell, Tanzeem Choudhury, Marta Hauser, John Kane, Michael Merrill, Emily A Scherer, et al. "CrossCheck: toward passive sensing and detection of mental health changes in people with schizophrenia." In *Proceedings of the 2016 ACM international joint conference on pervasive and ubiquitous computing*, pp. 886–897, 2016.

[WBS16]   Wenjin Wang, Albertus C den Brinker, Sander Stuijk, and Gerard De Haan. "Algorithmic principles of remote PPG." *IEEE Transactions on Biomedical Engineering*, **64**(7):1479–1491, 2016.

[Weg96]   Peter Wegner. "Interoperability." *ACM Computing Surveys (CSUR)*, **28**(1):285–287, 1996.

[WF01]   Lianne J Woodward and David M Fergusson. "Life course outcomes of young people with anxiety disorders in adolescence." *Journal of the American Academy of Child & Adolescent Psychiatry*, **40**(9):1086–1093, 2001.

[who]   "Ageing and health.".

[WK10]   Diane M Wrisley and Neeraj A Kumar. "Functional gait assessment: concurrent, discriminative, and predictive validity in community-dwelling older adults." *Physical therapy*, **90**(5):761–773, 2010.

[WKF16]   Fabian Wahle, Tobias Kowatsch, Elgar Fleisch, Michael Rufer, Steffi Weidt, et al. "Mobile sensing and support for people with depression: a pilot trial in the wild." *JMIR mHealth and uHealth*, **4**(3):e5960, 2016.

[WPB16]   Cylie M Williams, Verity Pacey, Pauline B de Bakker, Antoni J Caserta, Kelly Gray, and Raoul HH Engelbert. "Interventions for idiopathic toe walking." *The Cochrane Database of Systematic Reviews*, **2016**(10), 2016.

[WTC10]   Cylie M Williams, Paul Tinley, and Michael Curtin. "Idiopathic toe walking and sensory processing dysfunction." *Journal of foot and ankle research*, **3**(1):1–6, 2010.

[WTL17]   Suhang Wang, Jiliang Tang, and Huan Liu. "Feature Selection.", 2017.

[XHA12]   Wenyao Xu, Ming-Chun Huang, Navid Amini, Jason J Liu, Lei He, and Majid Sarrafzadeh. "Smart insole: A wearable system for gait analysis." In *Proceedings of the 5th international conference on pervasive technologies related to assistive environments*, pp. 1–4, 2012.

[XLL13]   Chenren Xu, Sugang Li, Gang Liu, Yanyong Zhang, Emiliano Miluzzo, Yih-Farn Chen, Jun Li, and Bernhard Firner. "Crowd++ unsupervised speaker count with smartphones." In *Proceedings of the 2013 ACM international joint conference on Pervasive and ubiquitous computing*, pp. 43–52, 2013.

[YCL19]   Yanni Yang, Jiannong Cao, Xiulong Liu, and Xuefeng Liu. "Multi-breath: Separate respiration monitoring for multiple persons with UWB radar." In *2019 IEEE 43rd Annual Computer Software and Applications Conference (COMPSAC)*, volume 1, pp. 840–849. IEEE, 2019.

[YFN19]   Ashkan Yousefpour, Caleb Fung, Tam Nguyen, Krishna Kadiyala, Fatemeh Jalali, Amirreza Niakanlahiji, Jian Kong, and Jason P Jue. "All one needs to know about fog computing and related edge computing paradigms: A complete survey." *Journal of Systems Architecture*, **98**:289–330, 2019.

[ZXL19]   Hanbin Zhang, Chenhan Xu, Huining Li, Aditya Singh Rathore, Chen Song, Zhisheng Yan, Dongmei Li, Feng Lin, Kun Wang, and Wenyao Xu. "Pdmove: Towards passive medication adherence monitoring of parkinson's disease using smartphone-based gait assessment." *Proceedings of the ACM on interactive, mobile, wearable and ubiquitous technologies*, **3**(3):1–23, 2019.